ENHANCED LAND SUBSIDENCE AND SEDIMENT DYNAMICS IN GALVESTON BAY- IMPLICATIONS FOR GEOCHEMICAL PROCESSES AND FATE AND TRANSPORT OF CONTAMINANTS

A Thesis

by

MOHAMMAD ALMUKAIMI

Submitted to the Office of Graduate Studies of
Texas A&M University
in partial fulfillment of the requirements for the degree of

MASTER OF SCIENCE

Chair of Committee,	Timothy Dellapenna
Committee Members,	Peter Santschi
	Patrick Louchouarn
	Chris Houser
Head of Department,	Piers Chapman

August 2013

Major Subject: Oceanography

ABSTRACT

Galveston Bay is the second largest estuary in the Gulf of Mexico. The bay's watershed and shoreline contains one of the largest concentrations of petroleum and chemical industries in the world, with the greatest concentration within the lower 15 km of the San Jacinto River/Houston Ship Channel (SJR/HSC). Extensive groundwater has been withdrawn to support these industries and an expanding population has resulted elevated land subsidence, with the highest land subsidence in the lower SJR/HSC, of over 3 m (3 cm yr^{-1}) and has decreased seaward throughout the bay to 0.6 cm yr^{-1} near Galveston Island. Mercury (Hg) contamination is well documented throughout the bay's sediments. Sediment vibra-cores were collected throughout the bay systems. ^{210}Pb and ^{137}Cs geochronologies from these cores was used to determine sedimentation rates and correlated to Hg profiles to estimate input histories. Relative Sea Level Rise (RSLR) is the sum of eustatic sea level rise and land subsidence. The results show sedimentation rates are high in areas with high rates of RSLR and the rates are of the same order of magnitude, however, in general, sedimentation rates are as much as 50% of RSLR, indicating that sedimentation has not kept pace with land subsidence, although they have the same relative order. Hg core profiles were correlated with radioisotope geochronologies and show significant input of Hg beginning around 1940, with a peak around 1971, and a dramatic drop off in concentration afterwards, demonstrating it to be a valuable geochronology tool. Hg concentrations were found to be dramatically higher proximal to the SJR/HSC and progressively decreasing seaward and to distal parts of the bay.

ACKNOWLEDGEMENTS

I would like to thank my committee chair, Dr. Timothy Dellapenna, and my committee members, Prof. Peter Santschi, Dr. Patrick Louchouarn, and Dr. Chris Houser, for their guidance and support throughout the course of this research. I would also like to thank Dr. Bob Presley and Dr. Gary Gill for their support and the valid advises especially on mercury.

Thanks also go to my friends and colleagues and the department faculty and staff for making my time at Texas A&M University a great experience. I also want to extend my gratitude to the people at the coastal geology laboratory, for providing the survey instrument, and to the entire TAMUG graduate student who were willing to participate in the study.

This thesis is dedicated my mother and father for their encouragement and to my lovely and wonderful wife for her patience, love, encouragement, and support provided.

NOMENCLATURE

^{137}Cs	Radioactive Cesium	
^{210}Pb	Radioactive Lead	
AR	Anthropogenic	
CRM	Certified Reference Materials	
EPA	Environmental Protection Agency	
GBNEP	Galveston Bay National Estuary Program	
GOM	Gulf of Mexico	
GPS	Global Positioning System	
GSLR	Global Sea Level Rise	
Hg	Mercury	
HGSD	Houston Galveston Land subsidence District	
HSC	Houston Ship Channel	
InSAR	Interferometric Synthetic Aperture Radar	
RSLR	Relative Sea Level Rise	
SJR	San Jacinto River	
USGS	United State Geological Survey	
α	Slope defined by a regression through the data	
^{210}Pb$_{xs}$	excess ^{210}Pb concentration	dpm g^{-1}
d	Thickness of sediment	cm
D_{pk}	Peak concentration of ^{137} Cs	dpm g^{-1}
Hg flux	Mercury Flux	ng m^{-2} yr^{-1}
Hg Inv	Mercury inventory	ng m^{-2}
m_d	Mass of dried sediment	g
m_w	Mass of water	g
ρ_s	Density of sediment (2.65)	g cm^{-3}
ρ_w	Density of the pore water	g cm^{-3}
RSD	Relative Standard Deviation	%

S	Pore water salinity	dimensionless
S	Sedimentation rate	cm yr^{-1}
S_{Avg}	Average sediment accumulation rate	cm yr^{-1}
T	Time difference to 1963	year
T-Hg	Total Dry Mercury	ng g^{-1}
λ	Decay constant of ^{210}Pb (0.031).	$year^{-1}$
ϕ	Porosity	dimensionless
z	Corrected depth	cm

TABLE OF CONTENTS

Page

LIST OF FIGURES

Page

LIST OF TABLES

1. INTRODUCTION

The Galveston Bay system is very complex and provides valuable ecological and economic resources. Galveston Bay is the seventh largest estuary in the United States (USA) and includes the San Jacinto River/Houston Ship Channel (SJR/HSC) the busiest shipping lane in North America (Figure 1). The Galveston Bay watershed contains Houston, the fourth largest city and fifth largest metropolitan area in the US and contains one-third of the US petroleum refining capacity located along its shores (Figure 2), along with associated chemical industries. Moreover, Houston Port is the second largest port in the US and the eighth in the world with the highest foreign tonnage in the Americas [EPA, 2007]. As a result of these industries and anthropogenic activities, there has been extensive land subsidence and extensive contamination of sediments, especially in SJR/HSC. Land subsidence was noticed in the early 1900's after groundwater, oil and gas were extracted (Figure 3). Between the 1906 and 1943, the period when the Houston petroleum industry was initially being developed, land subsidence was localized with a maximum of 0.18 m (0.48 cm yr^{-1}). Beginning around 1940 with the onset of WWII and during the post-war industrial boom, there was a rapid expansion of refineries along the SJR/HSC along with the associated boom in the population of Houston. As a result, land subsidence started to become a more regional problem (Figure 4) [*Coplin and Galloway*, 1999; *HGSD*, 2013; *USGS*, 2002].

In the Houston-Galveston Bay area, land subsidence has caused significant loss of habitats and salt marsh erosion during this period [*Lester and Gonzalez*, 2011; *Ravens et al*, 2009]. Moreover, land subsidence has increase the intensity and frequency of flooding and cost millions of dollars. Groundwater pumping and the development of the oil and gas fields are the main mechanism, which causes the area to subside and, water, and sediment to contaminates through points and non-point sources [*GBNEP*, 1992; *GBNEP*, 1994; *HGSD*, 2013; *USGS*, 2002; *Gardinali*, 1996].

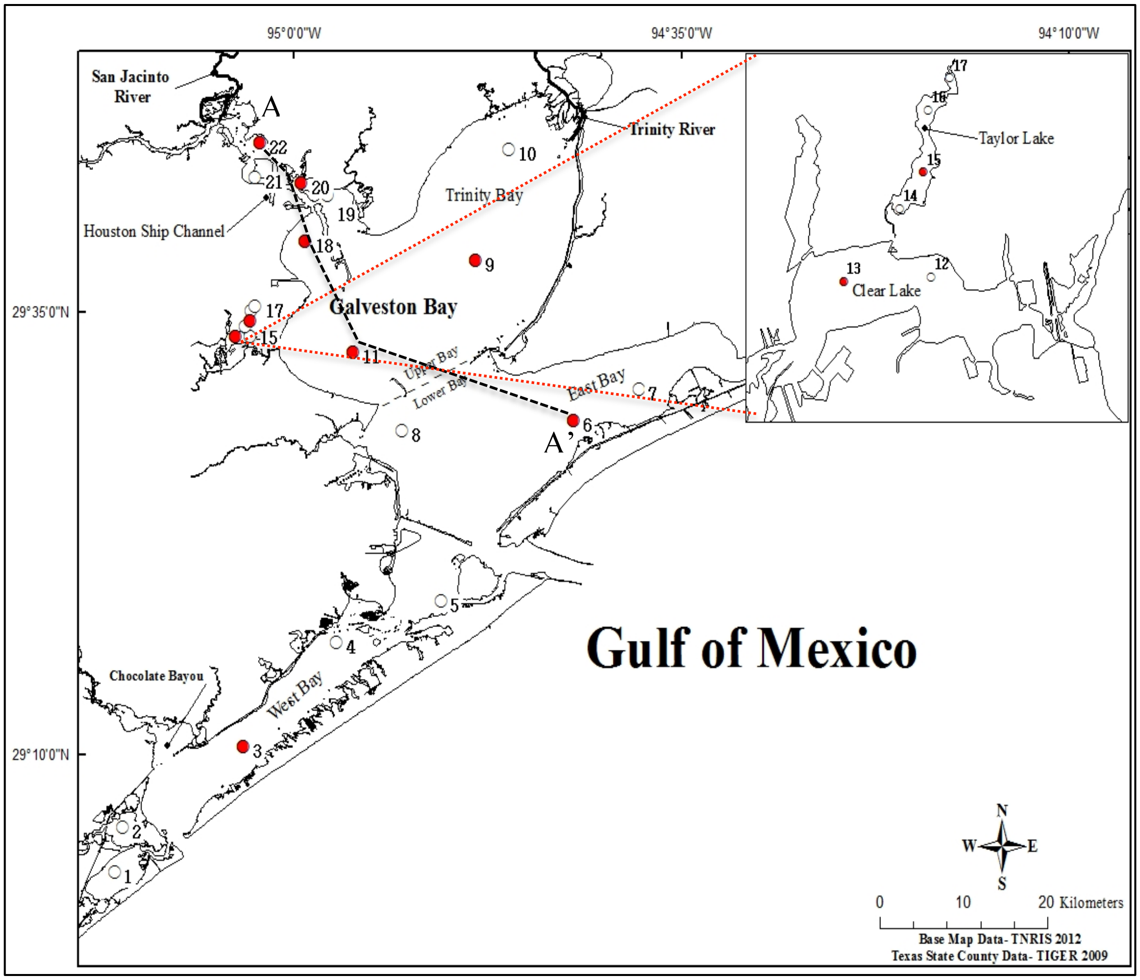

Figure 1. Samples location in Galveston Bay area. Red: selected core location. White: not sampled cores. Cross section A-A'.

Much of the research conducted on SJR/HSC-Galveston Bay land subsidence issue has focused on quantifying rates and the risks associated with it as it pertains to land loss, land usage, and other societal issues. However, the question of whether sedimentation within the bay has kept pace with the enhanced bay bottom subsidence and the implication of this to fate and transport of contaminants, nutrients and organic matter within the bay system has not been addressed.

Galveston Bay is a coastal plain estuary which formed due to the submergence of the incised Trinity and San Jacinto River valleys, beginning around 9,000 yBP, during the Holocene rise in sea level and reached its current configuration around 2,500 yBP (*Rodriguez et al*, 2005). In general, estuaries exist and are maintained because a balance is achieved between sediment flux, accommodation space and hydrodynamics [*Dalrymple et al*, 1992; *Rodriguez et al*, 2005; *Nichols*, 2009; *Bianchi*, 2007]. Accommodation space is created by sea-level rise, subsidence or a combination of both. If the sediment supply is sufficient, the space will be filled until a hydrodynamic equilibrium is achieved. If the sediment supply cannot keep pace with the formation of accommodation space, than the estuary will deepen. If sediment supply is in excess of that which is needed to fill the accommodation space and that which can be removed by the hydrodynamics, the estuary will fill and transition into a delta.

Mercury is very toxic, it is transformed to methylmercury in the marine environment and bioaccumulates in marine organism and poses a hazard when these organisms are consumed by humans [*Liu et al*, 2012; *Bank*, 2012]. Studies have shown that there is a very high concentration of mercury in Houston Ship Channel, however, the concentration in other areas of the bay are much lower [*Harmon*, 2003; *Lester and Gonzalez*, 2011]. The overall purpose of this study is to determine if sedimentation within the Galveston Bay system, including the SJR/HCS kept pace with the elevated land subsidence and elevated sea level rise experienced in the past century. This has been accomplished through analyses of a combination of ^{210}Pb and ^{137}Cs geochronologies from sediment cores. ^{210}Pb is a naturally occurring radioisotope with a 22 year half life, ^{137}Cs is a bomb produced isotope which did not exist in measureable quantities in nature prior to 1954 [*Nittrouer et al*, 1979; *Santschi et al*, 1999; *Bianchi*, 2007; *Dellapenna et al*, 1998]. Profiles of Hg concentrations are used to investigate the history of Hg inputs to the system, to test the utility of Hg input as an additional geochronology tool. In addition, the distribution of Hg in the sediments have been used to assess the implications of enhanced subsidence driven sedimentation on the fate and transport of particle bound contamination within estuarine systems. To accomplish this, four hypotheses have been tested:

1. The sedimentation rate reflects relative sea-level rise for the past 100 years in Galveston Bay.
2. Areas with higher sedimentation rate have higher inventories of mercury.
3. Total mercury concentration in sediments profile decrease with distance from the estuary to the open sea.
4. Mercury can be used as a geochronology tool in Galveston Bay.

1.1 Background

1.1.1 Study area - Galveston Bay

Galveston Bay (Figure 1) is the second largest estuary in the Gulf of Mexico and the seventh largest in the United States, with a surface area of 1554 km^2. The bay is located northeast to the Gulf of Mexico. Galveston Bay is divided to four major sub-bays, Galveston, Trinity, West and East Bay. Fresh water input to the Bay is primarily from the Trinity River and San Jacinto River, with Chocolate Bayou as a minor source (Figure 1). Galveston Bay is a turbid estuary with an average depth of 2 m [*Wen et al*, 1999]. The major tidal inlet in this system is located between Galveston Island and Bolivar Peninsula. Sediment fluxes of nutrients and trace metals are very high within the bay area [*Lee et al*, 2011; *Santschi et al*, 2001].

The areas around the bay, especially around the SJR/HSC, are intensely industrialized with chemical and petrochemical plants (figure 2). One-Third of the oil refined in the United State is refined in the refineries along Galveston Bay. The net result of all of these industries is extensive anthropogenic environmental impacts, including: extensive land subsidence in upper bay and SJR/HSC [*USGS*, 2002; *Coplin and Galloway*, 1999], poor air quality-resulting from atmospheric fallout of particle bound contaminants and extensive contamination of sediments within the upper bay and SJR/HSC. Thus, as a result of the high concentration of industries along the bay's shores and the increase of population, many studies have found high concentrations of trace metals and toxic contaminants in SJR/HSC [*Wen et al*, 1999; *Morse et al*, 1993; *Santschi et al*, 2001]. *Harmon et al* (2003) found that there is a uniform distribution of trace metals in the surface sediment in Galveston Bay with exception of mercury which was high in in the SJR/HSC (200 ng g^{-1}), proximal to where a chlor-alkali plant is located (Patrick Bayou), and about 50 ng g^{-1} elsewhere. Mercury concentration in the bay ranged between 10 to 280 ng g^{-1} with a flux to the surface sediment of 13.6 ng cm^{-2} yr^{-1} [*Morse et al*, 1993; *Santschi et al*, 2001]. Even with the highly developed petroleum, petrochemical, and chemical industries along Galveston Bay, the concentration of trace metals in the water column and surface sediment is low and the system is no longer considered as a greatly polluted system [*Santschi et al*, 2001; *Wen et al*, 1999].

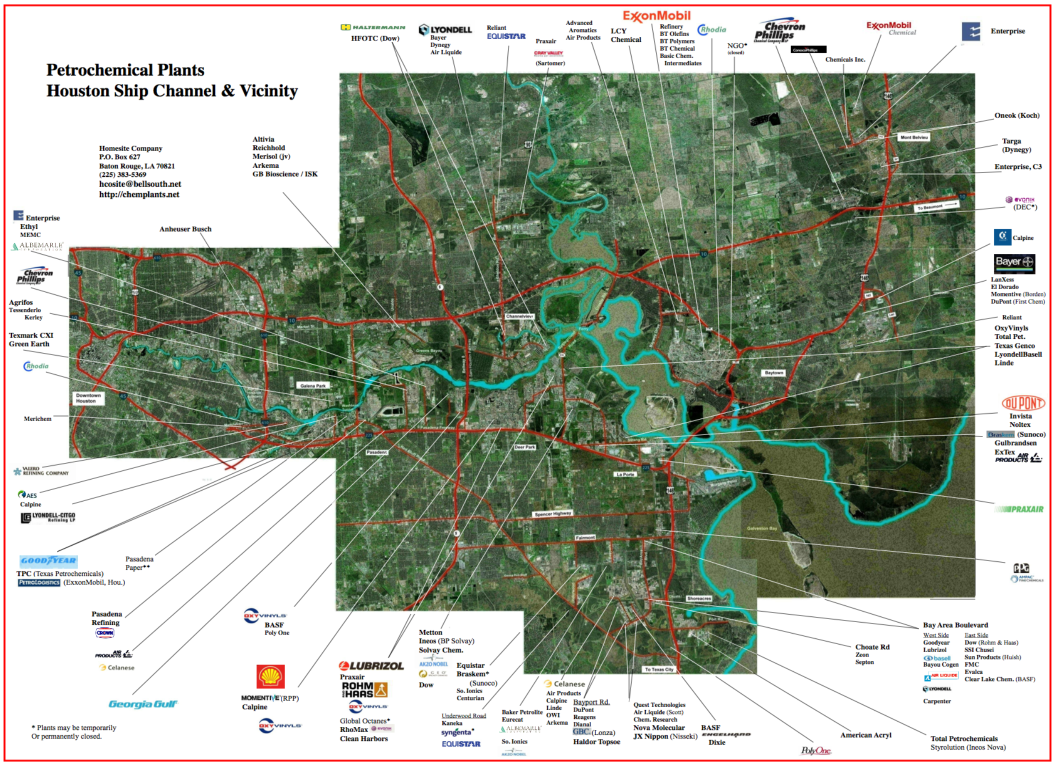

Figure 2. Map shows the location of most of the petrochemical plants in Houston Ship Channel and area around it [*ChemPlants*, 2013].

1.1.2 Land subsidence in Galveston Bay

Land subsidence can be defined as lowering or sinking of the land surface relative to the surrounding terrain [*Hu et al*, 2004; *Zilkoski et al*, 2003; *Kasmarek et al*, 2010]. Land subsidence can be caused by natural processes such as earthquakes, volcanoes, tectonic activities and sea level rise as well as human induces factors, most notably enhanced groundwater or other fluid withdraw [*Hu et al*, 2004]. Extensive land subsidence can negatively impact ecosystems, create wetlands losses, damage infrastructure, and increase flooding frequency [*Coplin and Galloway*, 1999; *USGS*, 2002; *Ravens et al*, 2009].

In Houston-Galveston Bay area, land subsidence is caused by groundwater pumping as well as by oil and gas extraction. This causes enhanced geostatic pressure and causes clay lattices to compact [*Coplin and Galloway*, 1999; *USGS*, 2002; *HGSD*, 2013]. Groundwater was the original primary source of water in Houston-Galveston Bay area. In 1897, the area experience a growth in population as a result of the discovery of oil, resulting in the opening of San Jacinto River section of the Houston Ship Channel (SJR-HSC) in 1914 and growth in industry along its banks (Figure 3). In the early 1900s, enhanced land subsidence began due to groundwater pumping and oil extraction and it was extensive in the early 1940, this ultimately lead to approximately 3 m of land subsidence throughout the 20th century (Figure 4), with greatest land subsidence centered around SJR-HSC and decreasing towards the south and east [*HGSD*, 2008; *USGS*, 2002].

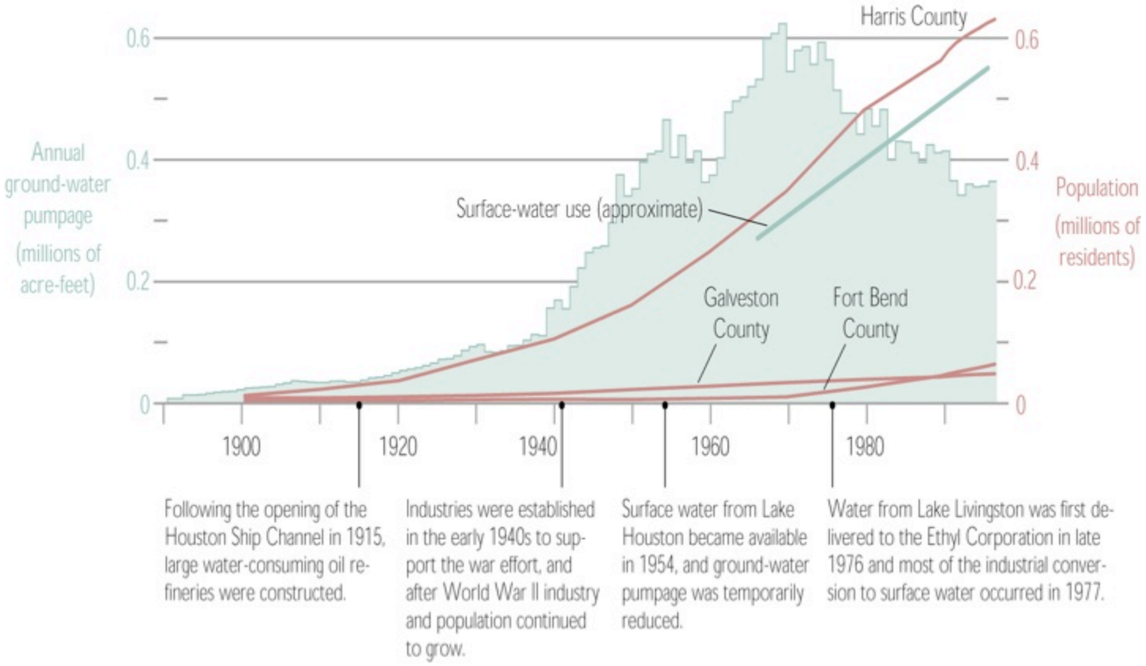

Following the opening of the Houston Ship Channel in 1915, large water-consuming oil refineries were constructed.

Industries were established in the early 1940s to support the war effort, and after World War II industry and population continued to grow.

Surface water from Lake Houston became available in 1954, and ground-water pumpage was temporarily reduced.

Water from Lake Livingston was first delivered to the Ethyl Corporation in late 1976 and most of the industrial conversion to surface water occurred in 1977.

(Compiled from Jorgenson, 1961; Gabrysch, 1987; and Harris-Galveston Coastal Subsidence District, 1996)

Figure 3. Annual groundwater pumping and number of population since early 1900 [*Coplin and Galloway*, 1999].

In Houston-Galveston Bay area, the land subsidence rate has been monitored using Global Positioning System (GPS) and Interferometric Synthetic Aperture Radar (InSAR). In 1954, ground water pumping was temporarily reduced when the surface water from Lake Houston became available. By 1977, most industries were using surface water from Lake Livingston, which reduced groundwater pumping. Land subsidence since then has been controlled and the rate has been reduced. The withdraw of groundwater within the regions of intense land subsidence are strongly regulated and within the metropolitan area, in general, reduced, resulting in an overall reduction in the land subsidence rate [*Coplin and Galloway*, 1999; *HGSD*, 2013; *USGS*, 2002; *Zilkoski et al*, 2003].

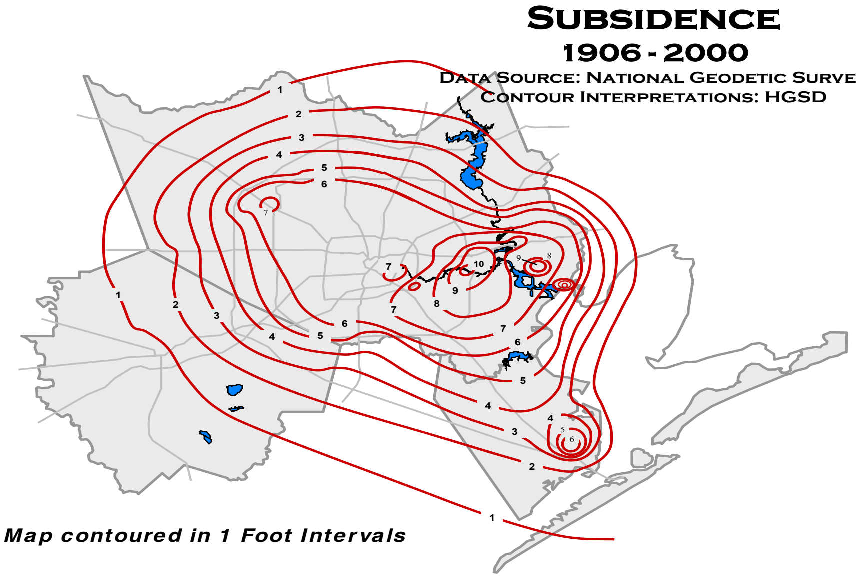

Figure 4. Contour map of land subsidence (feet) in Galveston Bay area between 1906 and 2000 [*HGSD,* 2008].

1.1.3 Mercury

Mercury (Hg) is a very toxic metallic element that occurs naturally in the Earth's biogeochemical systems [*Bank*, 2012]. There are many sources of mercury in the environment including both natural and anthropogenic sources and activities. Natural sources include volcanic activities and weathering of mercury bearing rocks. Anthropogenic emissions primarily come from coal combustion, fossil fuels, medical incineration and local waste combustion [*Liu et al*, 2012; *Sanders et al*, 2008]. Anthropogenic activities extracted mercury from deep reservoirs which changed the cycle of mercury and increased the total atmospheric concentration of Hg by a factor of three since the beginning of the 21st century or more specifically, the beginning of the industrialization period, and that caused increase in mercury deposition in the environment [*Bank*, 2012]. In the environment and the biogeochemical system, mercury has three primary categories and compounds: elemental mercury, inorganic mercury, and organic mercury. In the environment (figure 5), Mercury exists in three oxidation states:

metallic or elemental mercury (Hg (0)), mercurous (Hg (I)), and mercuric (Hg (II)). [*Liu et al*, 2012; *Bank*, 2012]. The organic (monomethylmerucy, CH_3Hg^+) and inorganic (Hg (II)) forms of mercury are the dominant forms in the aquatic environment, while the elemental Hg (0) is the primary form in the atmosphere. Most inorganic forms of mercury are in the salt phase, either white powder or crystals [*Clampet*, 2012]. Chloro complexes and chloride ($HgCl_2$) are the major inorganic mercury forms in seawater [*Sibley and Morgan*, 1977] and mercuric hydroxide ($Hg(OH)_2$) is the major form in low salinity estuarine systems [*Lockwood and Chen*, 1973]. In sediments, mercury is associated with humic matter and the major ore for mercury is cinnabar (HgS) and typically forms through hydrothermal intrusions [*Bank*, 2012]. It is essential to understand the relation between Hg and sulfide in estuarine systems in order to fully understand the Hg bioavailability and methylation processes that determine the fate of such toxic element [*Han et al*, 2007]. Mercury has many organic forms such as deimethlmercury, phenylmercury, ethylmercury, and methylmercury, which is the most toxic form of mercury and the most common form in the environment [*Clampet*, 2012]. In aquatic environments, the different forms of mercury can transform from one to the other. For example, the sulfate reducer bacteria (Desulfovibrio desulfuricans) transform the inorganic mercury into monomethylmerury (MMHg), which is strongly bioaccumulated in the ecosystem. ''This bacteria can transfer the methyl group from CH_3-tetrahydrofolate via methylcobalamin to Hg^{+2} in anzyme-mediatd reaction'' [*Neff*, 2002]. Methylmercury can easily bioaccumulate in organism and the concentration can be much higher than the surrounding water. Both biotic and abiotic processes can form Methylmercury in the environment [*Neff*, 2002; *Clampet*, 2012].

In general, the concentration level of methylmercury in sediment does not exceed 2% of the total mercury [*Bank*, 2012].

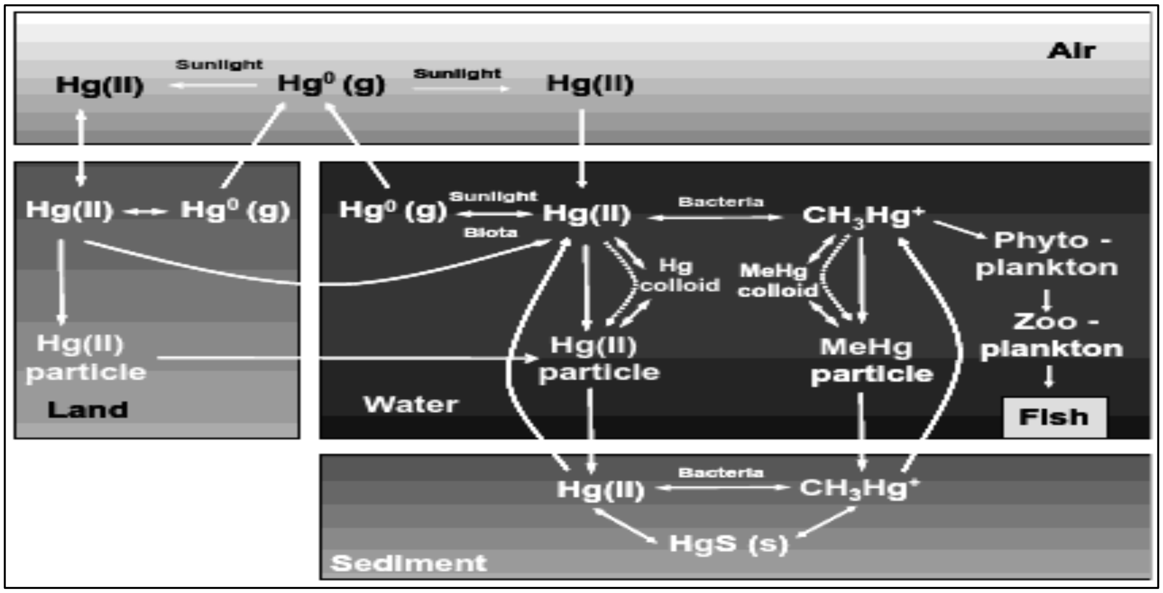

Figure 5: Mercury biogeochemical cycle in the environment [*Lasorsa et al*, 2012].

In the last 100 years, human activities have increased all around the world, and as a result, mercury has become one of the major global pollutants [*Liu et al*, 2012; *Bank*, 2012; *Di Leonardo et al*, 2006]. The toxicity of mercury depends on its chemical form, and due to the high toxicity of mercury, the biogeochemistry of this heavy metal in estuarine environments has been widely studied [*Shi et al*, 2010]. In estuarine and coastal systems, mercury concentrations (Hg) are much higher than open oceans due to anthropogenic activities [*Bank*, 2012]. Many studies have shown how the anthropogenic activities can affect the mercury concentration and distribution in the environment. Moreover, how radionuclides geochronology can be used to reconstruct the historical contaminant inputs in many estuaries. It is important to reconstruct the historical input for improving management strategies [*Di Leonardo et a*l, 2006; *Menounou and Presley*, 2003; *Sanders et al*, 2008; *Louchouarn and Lucotte*, 1998; *Figueres et al*, 1985; *Kading et al*, 2009]. For example, in Pearl River Estuary, China, total mercury concentration results show spatial and temporal variations within the sediments. The mercury concentration decreases toward the open ocean, which indicate that the anthropogenic activities in the estuary are the main sources of emission. ^{210}Pb was used as a dating technique to determine the historical changes in Hg concentration. The study concludes that the Hg fluxes and economic developments are well correlated in this system in the last three decades [*Shi et al*, 2010]. In estuarine water, mercury transportation and distribution is influenced by the complexation of mercury by DOM, colloidal coagulation, and particle scavenging. Sulfides are important binding sites for dissolved mercury in estuaries, which was suggested due to the conditional stability constants between mercury and natural ligands. The study demonstrates that dissolved mercury in Galveston Bay is complexed by natural ligands. The study shows that the natural ligands are responsible for dissolved mercury complexation in estuarine water [*Han et al*,2006]. Mercury in Galveston Bay and Corpus Christi Bay has a ‘‘nonconservative estuarine mixing behavior’’. The concentrations of mercury in Galveston Bay decrease towards the sea (with increasing salinity) and the filter-passing mercury have two distinct sources. Around 60% of the filter-passing mercury was bonded to colloidal material in Galveston Bay and the other proximal estuaries. The strong correlation between mercury (Hg) and Colloidal Organic Carbon (COC) indicate that the process affecting organic carbon concentration will affect the Hg cycling in estuaries [*Stordal et al*, 1996].

1.1.4 Radioisotope applications

Short-lived radioisotope geochronology, including natural radionuclide such as ^{210}Pb ($t_{1/2}$ = 22.3 yr, $E\gamma$= 46 KeV) and anthropogenic nuclide such as ^{137}Cs ($t_{1/2}$ = 30.2 yr, $E\gamma$= 662 KeV), has been used extensively to investigate sedimentary processes and sedimentary records in wide variety of aquatic and marine environments including estuaries [e.g. *Nittrouer et al*, 1979; *Santschi et al*, 1999; *Sharma et al*, 1987; *Dellapenna et al*, 1998; *Dellapenna et al*, 2003; *Yeager et al*, 2004]. In shallow environment, it is better to use more than one radionuclide to obtain precise information about sedimentation rates rather than relying on ^{210}Pb$_{xs}$ itself [*Santschi et al*, 1999; *Jason and Baskaran*, 2011]. Both ^{210}Pb and ^{137}Cs are used in this study to determine the sedimentation rate in Galveston Bay and to reconstruct the historical input of mercury in the bay for the last 100 years. For both isotopes, it is always assumed that the it has a very short residence time in the water compared to it is half-life time and that they are absorbed into fine-grained particles [*Dellapenna et al*, 1998; *Nittrouer et al*, 1979; Krishnaswami *et al*, 1971].

^{210}Pb is the final long-lived radionuclide (22.4 years) in the decay of ^{238}U in the earth's crust. The decay series of ^{238}U includes ^{226}Ra, which decay to ^{222}Rn, a noble gas, which then escapes into the atmosphere at a constant rate. The Radon atoms in the atmosphere subsequently decay through a series of short-lived radionuclides to produce unsupported components of ^{210}Pb activity. ^{210}Pb is primarily removed from the atmosphere by washout of wet and dry fallout. $^{210}\text{Pb}_{xs}$ then is deposited in the snow, ice of glaciers, lakes, and oceans. The half-life time of ^{210}Pb allows the determination of sedimentation rate back 50-100 years (about five half-life times) [*Bianchi*, 2007; *Faure and Mensing*, 2005; *Baskaran and Naidu* 1995; *Nittrouer et al*, 1979].

^{137}Cs is used as an impulse tracer and it is anthropogenically introduced into the environment via the atmospheric testing of the nuclear weapons and releases from nuclear power facilities (both locally and regionally). The atmospheric weapons testing beginning in 1952 and ^{137}Cs was deposited in the environment through processes similar of ^{210}Pb. In 1963, an extensive nuclear testing caused a well establish peak of ^{137}Cs in the sediment profile. Either the maximum fallout or the first appearance in sediment enables the establishment of sediment chronologies [*Van Metre et al*, 2004; *Santschi et al*, 1999 ; *Jason and Baskaran*, 2011].

2. METHODS

2.1 Data collection and core processing

A total of 22 sediment cores (Fig 1) were collected from Galveston Bay on four cruises (June 15, July 27, August 1 and 8, 2012) using viba-corer with 7.62 cm diameter aluminum core barrels and 1 to 3 m of sediment recovered. The recovered cores were sealed immediately and were stored upright in the boat and then in the refrigerator (∿ 4°C) for further processing and analyses. The core locations were chosen at sites where there is no history of dredging and where they appears to be representative depositional setting. These locations cover most of the bay, including the lower reachs of the SJR-HSC. In the laboratory, each core was cut in half lengthwise. One half of the core was X-rayed, photographed and visual descriptions of the core lithology were recorded and then stored in the core was placed in refrigerated storage (archive) for a future reference. The other half of the core was sectioned at 1 cm intervals for the upper 10 cm, every 2 cm for 10 cm to 50 cm, and every 5 cm thereafter. Some of the sampling halves of the cores were sectioned every 1 cm throughout. Wet samples were extracted from the core and stored in labeled whirl-pak bags for water content, grain size analyses, and ^{137}Cs geochronology. The dried samples were ground for total mercury concentration, and ^{210}Pb geochronology analyses via alpha spectroscopy (see below).

2.2 Water content

Samples from various depths in these cores were immediately placed in pre-weighed aluminum tins and kept in an oven for at least 24 hours, and then re-weighed to determine water content. The porosity was calculated from the water content by estimating the salt content and the sediment density of 2.65 g cm^{-3}. Porosity (ϕ) was calculated using the equation:

$$\emptyset = (m_w/\rho_w)/(m_w/\rho_w + ((m_d - (S * m_w)))/\rho_s) \quad (1)$$

Where (m_w) is the mass of water, (ρ_w) is the density of the pore water, (m_d) is the mass of dried sediment plus salt, (S) is the pore water salinity, and (ρ_s) is the density of sediment particles, which is the density of pure mineral phase of quartz [*Burdige*, 2006].

The porosity values were used to calculate the corrected depths for the ^{137}Cs and ^{210}Pb geochronology. The equation used to calculate the corrected depth in centimeter is:

$$\text{Corrected Depth} = \text{Cumulative Mass} / (((1 - \emptyset) * \rho_s)) \quad (2)$$

2.3 Grain size analyses

Wet sediment samples at 5 cm depth intervals from cores were analyzed in the laboratory for grain size distribution using Malvern Mastersizer 2000. A laser diffraction technique is used to determine the particle size by measuring the light scattered intensity from the dispersed particles in a liquid medium. About 2-4 g of the wet samples were homogenized and placed in a 100 mL glass jar. Ten milliliters (10 mL) of 5.5 g L^{-1} of sodium hexametaphosphate were added to the sediment samples as a dispersant solution and approximately 20 mL of deionized water was added to the jar. To disaggregate the samples, the jars were sonicated for 30 minutes at 25 °C and frequency of 40 kHz. Because the Malvern instrument has a range of 0-2000 μm, all samples were wet sieved after sonication in a 2 mm sieve into 200 mL glass jar. The larger fraction of the samples, such as shells, were placed in pre-weighed aluminum tins and kept in an oven for at least 24 hours, and then re-weighed to determine the final grain size distribution. The jar with samples of < 2mm were filled with deionized water to a volume of 200 mL. The jars were placed on a stir plate to mix the samples. Ten milliliters (10 mL) from the stirring samples was pipetted into pre-weighed aluminum tins and dried in the oven for at least 24 hours, and then re-weighed for the weight percentage calculation. The stirring samples were pipetted into the instrument until the obscuration level was reached. Then, the instrument measured the fraction of sand, silt, and clay within each sample three times and then averaged them. The results obtained from the Malvern in addition to the 10 ml sample that was removed, with the percentage of the fraction more than 2 mm were added to calculate the final fraction of gravel, sand, silt, and clay.

2.4 Radioisotope analyses - ^{210}Pb and ^{137}Cs

Wet and dry sediment samples for geochronology analyses were removed form the whirl-pak bags and homogenized to determine the activity of both ^{210} Pb and ^{137} Cs. For ^{137} Cs analyses ($t_{1/2}$ = 30 yr, $E\gamma$= 662 KeV), wet samples were placed in 50 x 9 mm and 60 x 15 mm petri dishes and sealed using electrical type. Each sediment sample was counted for 1-2 days using a semi-planar intrinsic germanium detector coupled with Canberra DSA-1000 16K multichannel analyzer. Two radioactive standards (NIST, SRM 4357 and Cs-137 standard FF-294, Isotopes Products Laboratories) were used on each detector to determine the efficiency factors at the required gamma ray energy. The net counts of each sample were converted to activity by using the efficiency factor and the wet weight of each sample. Sedimentation rate from ^{137} Cs can be calculated from the following equation: $S = (D_{pk} / T)$ where (S) is the sedimentation rate (cm yr^{-1}) , (D_{pk}) is the peak concentration of ^{137} Cs which occurs in 1963, and (T) is the time difference to 1963 (50 years for this study). The activity of ^{210} Pb ($t_{1/2}$ = 22.3 yr, $E\gamma$= 46 KeV) was measured indirectly using its granddaughter ^{210} Po where they are assumed to be in secular equilibrium following the methods described by *Nittrouer et al* [1979] and *Santschi et al* [1999]. Dry sediment samples at 5 cm intervals were pulverized, homogenized and wet sieved through a 38 μm sieve using deionized water. The smaller fraction was used because clay and silt particles have a large surface area, which allow them to absorb large concentrations of radioisotopes such as ^{210} Pb [*Nittrouer et al,* 2007]. Then, approximately 1 g of the smaller fraction of each sample were placed in Teflon beakers and spiked with 0.25 μl of known activity of ^{209} Po tracer to assess the recovery of ^{210} Po. The samples were then digested with 15 ml of concentrated HCl and HNO_3, and 10 ml of HF. For some samples, HF was not used. The Teflon beakers were placed on hotplates to near dryness. After dryness, 15 ml of HCl and $HNO_{3,}$ were added and the same procedure was repeated. Then, 15 ml of HCl was added and the Teflon beakers were baked to near dryness. Then, 50 ml of 1.5 N HCl was added to the sediment samples and ascorbic acid was added and stirred to the leachate to complex the free Fe(III). Silver planchets with one side exposed (1 cm^2) were placed to each leachate along with a magnetic stir bar. The solution was then stirred for about 12 hours and both ^{209} Po and ^{210} Po were electroplated onto the silver planchets. The silver planchets were removed and counted for 24 hours by alpha spectroscopy using Canberra surface barrier detector. The activity of ^{210}Pb was obtained from the counts ratio of the Po isotopes and the relative activity of the spiked sample. Excess ^{210}Pb ($^{210}Pb_{xs}$), can be calculated as the difference between total activities and supported activities. The supported activity can be determined from constant ^{210}Pb activities at depth and/or ^{226}Ra activities. In order to calculate the sedimentation rate using $^{210}Pb_{xs}$, some assumptions need to be considered, such the flux of the $^{210}Pb_{xs}$ is constant at the sediment-water interface, it is chemically immobile, and over the depth interval the particle reworking rates are negligible [*Santschi et al*, 2001; *Sharma et al*, 1987]. So from a constant sediment accumulation rate and specific activity of the radioisotopes, When ^{210}Pb buried, it decay exponentially and the following equations used to calculate the sedimentation rate are:

$$[^{210}Pb_{xs}\,(z)] = [^{210}Pb_{xs}\,(0)]\ \exp\,(-\alpha z) \tag{3}$$

$$S = (\lambda/\alpha) \tag{4}$$

Where [$^{210}Pb_{xs}$ (z)] and [$^{210}Pb_{xs}$ (0)] represent excess ^{210}Pb concentration at the corrected depth z and at sediment interface, z = corrected depth in cm, (*S*) = linear sedimentation rate (cm y^{-1}); (λ) = decay constant of ^{210}Pb (0.031 $year^{-1}$). Alpha (α) = the slope defined by a regression through the data. The slope of the line, through data, ln [^{210}Pbxs (dpm g^{-1})] is plotted as the function of sample depth [*Dellapenna et al*, 1998; *Santschi et al*, 1999; *Santschi et al*, 2001].

2.5 X-radiography

The X-radiographs of the sediment cores were taken using MinX-Ray HF100+ Amorphous Silicon Imaging System 4030R, X-Ray unit at an energy level of 60 kV exposure time of 1/20 seconds.

2.6 Mercury analysis

For the analysis of total mercury concentration in the sediments, approximately 100 mg of dry and homogenized pulverized sediment samples at 5 cm intervals were analyzed using Direct Mercury Analyzer (DMA-80, milestone srl, Italy) which is complaint with U. S. EPA Method 7473 (Mercury in solids and solutions by thermal decomposition, amalgamation, and atomic absorption spectrophotometry)[*EPA*, 1998] . The dry samples were thermally decomposed in a controlled heating furnace to liberate mercury from the sediment. By a continuous flow of oxygen, the decomposition products were carried to a hot catalyst at 615 °C, which reduced all mercury species to the elemental form [Hg (0)] and trapped halogens, nitrogen, and sulfur oxides. Vapor mercury is then carried along with the oxygen to a gold amalgamator, which selectively collected it. Then the amalgamator was heated up to 900 °C, which released the mercury vapor, and the flowing oxygen carried the vapor mercury to hot cuvette cells 125°C (atomic absorption spectrometry) which quantified the absorption of elemental mercury at 253.7 nm wavelength as a function of mercury concentration [milestone, 2013; EPA, 1998]. The DMA-80 was calibrated using prepared standard solutions of mercury and the calibration curve was verified with Certified Reference Materials (CRM). Four standard solutions of mercury from inorganic ventures were used at different concentrations of mercury [0.1ppm Hg preserved in 3.7% HCl , 1ppm, 10 ppmHg preserved in 10% HCl and 100 ppm Hg preserved in 10% HNO] to calibrate the instrument for its full range. The 0.1 ppm aqueous standard was prepared using Milli-Q water by diluting 100 ppm mercury standard and transferred into amber glass bottles. All the standard solutions of mercury were preserved in the refrigerator to minimize the loss of mercury. Due to the loss of mercury as a result of chemical interaction between the acids and the nickel boats, quartz boats were used instead to calibrate the DMA-80. In order to ensure precision, reliability, accuracy and consistency of the sediment samples for the total Hg, three Certified Reference Materials (CRM) (MESS-3 Marine sediment [0.091 ± 0.009 ppm, National Research Council of Canada], NIST 2702 Inorganics in Marine sediment [0.4474 ± 0.0069 ppm, National Institute of Standards and Technology], and PACS-2 Marine sediment [3.04 ± 0.2 ppm, National Research Council of Canada]) were used representing a different Hg range. Once the instrument was calibrated with liquid standard solution, the calibration curve was verified with the three CRM. If the Hg concentration results were within the certified range for the standards, sediment samples along with the CRM were analyzed otherwise a new calibration curve would be obtained. Certified Reference Materials (CRM), blank to ensure no Hg is carried over the samples and duplicates to check the reproducibility were analyzed every 10 samples to ensure accuracy. The results obtained from the CRMs were excellent and in good agreement within the certified range with an average recovery rate for MESS-2 of 96 % ± 10 % (Mean ± RSD, n = 50), NIST 2702 (96 % ± 7 % (Mean ± RSD, n = 43), and PACS-2 (95 % ± 11 % (Mean ± RSD, n = 36).

3. RESULTS

Total Hg concentration, grain size distribution, excess ^{210}Pb activity, depth of maximum ^{137}Cs activity and x-radiographs were determined for a total of 9 core. Porosity and core photographs for each core are in appendix A. All profiles are shown with consistent depth scales (140 cm). Table 1 and 2, contains all the results obtained from Hg concentration and accumulation rates for all of the cores used in this study.

3.1 Core 3 – West Galveston Bay (WGB)

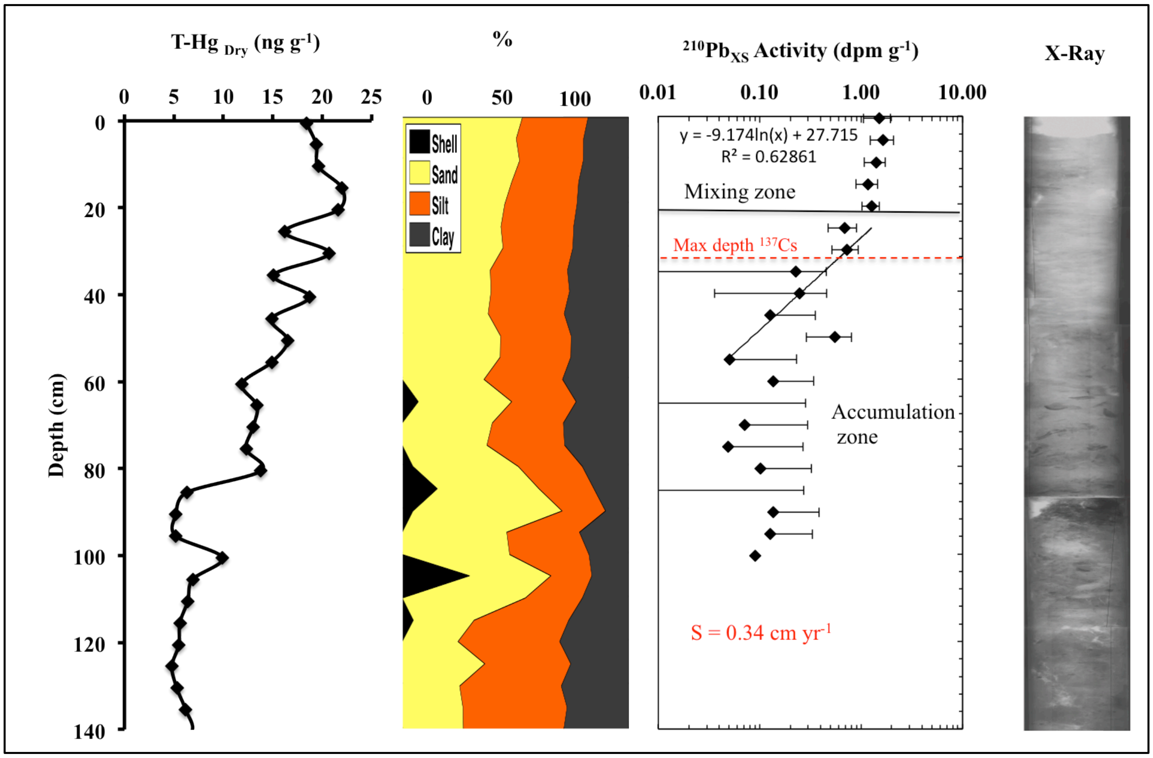

Figure 6. Vertical profile of total Hg concentration, grain size distribution, excess ^{210}Pb activity and X-ray for core collected in West Galveston Bay.

Table 1. Core locations, Average surface Hg concentration for the upper 5cm (S-Hg C), maximum Hg concentration (max Hg C), depth of maximum anthropogenic (AR) Hg concentration, depth where Hg reaches background, total and anthropogenic (AR) inventory of Hg for the upper 140 cm (T-Hg Inv; AR Hg Inv), present-day flux of Hg to the surface sediment (S-Hg flux)

	Latitude	Longitude	S-Hg C (ng g^{-1})	Max Hg C (ng g^{-1})	Depth of max AR Hg C (cm)	Depth of Hg Background (cm)	T-Hg Inv (ng m^{-2})	AR Hg Inv (ng m^{-2})	S-Hg flux (ng m-2 yr^{-1})
Core 3	29.174161 N	95.055394 W	18.9	22	N/A	N/A	1646	N/A	5.7
Core 6	29.481100 N	94.699469 W	14.55	30.8	N/A	N/A	2169	N/A	4.1
Core 9	29.631431 N	94.804969 W	52.55	54.6	5.5	21	2212	717	6.1
Core 11	29.545369 N	94.937464 W	47	56.8	N/A	116	3325	1478	65.5
Core 13	29.559783 N	95.064183 W	47.6	61.4	60.5	95.5	2576	2216	26.4
Core 15	29.574911 N	95.048233 W	47.85	65.5	45.5	80.5	2148	1573	17
Core 18	29.649886 N	94.988589 W	24.95	104.3	61	96	3521.5	2452.8	27.2
Core 20	29.704539 N	94.992633 W	40.85	146.8	96	N/A	6521.3	N/A	92.5
Core 22	29.742389 N	95.037833 W	157.85	2374.4	76	131	23228	22849	144.6

Table 2. Average sediment accumulation rate (S_{Avg}) obtained from ^{210}Pb and ^{137}Cs, Land Subsidence Rate (LSR) calculated between 1906 – 2000, Difference between ^{210}Pb & LSR, Relative Sea-Level Rise (RSLR), and Difference between ^{210}Pb & RSLR

	^{210}Pb S_{Avg} (cm yr^{-1})	^{137}Cs S_{Avg} (cm yr^{-1})	LSR (cm yr^{-1})	Difference between ^{210}Pb & LSR (%)	RSLR (cm yr^{-1})	Difference between ^{210}Pb & RSLR (%)
Core 3	0.34	0.29	0.3	13	0.47	-38
Core 6	0.53	0.58	0.3	77	0.47	11
Core 9	0.29	0.28	0.47	-38	0.64	-121
Core 11	1.55	3.3	1.6	-3	1.77	-14
Core 13	1.5	1.068	1.8	-13	1.97	-25
Core 15	1.1	2.55	1.87	55	2.04	30
Core 18	1.4	0.7	1.9	-26	2.07	-48
Core 20	3.2	N/A	2.9	10	3.07	4
Core 22	1.8	1.6	2.4	-25	2.57	-43

For each core, a background concentration was determined from constant Hg concentration with depth. The total mercury concentration profile obtained from Core 3 (figure 6), West Galveston Bay, shows Hg concentrations within the background range fluctuating between 4-22 ng g^{-1} and concentrations decrease with depth. Due to this low concentration of Hg in this location, it was difficult to distinguish between pre- and post contamination concentrations of Hg.

The grain size profile is shown as a percentage of shell, sand, silt, and clay. In general, the sand composition in this location ranges between 40% and 50%. At a depth of around 60 cm, there is an increase in the shell fraction. At depths below 120 cm, there is a decrease is sand fraction and an increase in silt and clay fraction. The relative high sand fraction is related to the location of the coring site. The coring site is in a back-bay environment between Galveston Island and the mainland.

West Galveston Bay has experience a land subsidence rate of about 0.3 cm yr^{-1} between the periods of 1906 and 2000. The profile of excess ^{210}Pb show a mixed layer in the upper 20 cm, with a consistently activity between 1.1 -1.6 dpm g^{-1} and decrease logarithmically with depth. The X-radiograph shows physical laminations with a few small burrows providing minor evidence of bioturbation in the upper 20 cm of the core. Sediment accumulation rate of 0.34 cm yr^{-1}, was calculated based on the decreasing of the ^{210}Pb activity between 20 and 55 cm. The maximum depth of ^{137}Cs activity (red dished line) was at 35 cm, which indicates a sediment accumulation rate of 0.29 cm yr^{-1}.

3.2 Core 6 – East Galveston Bay (EGB)

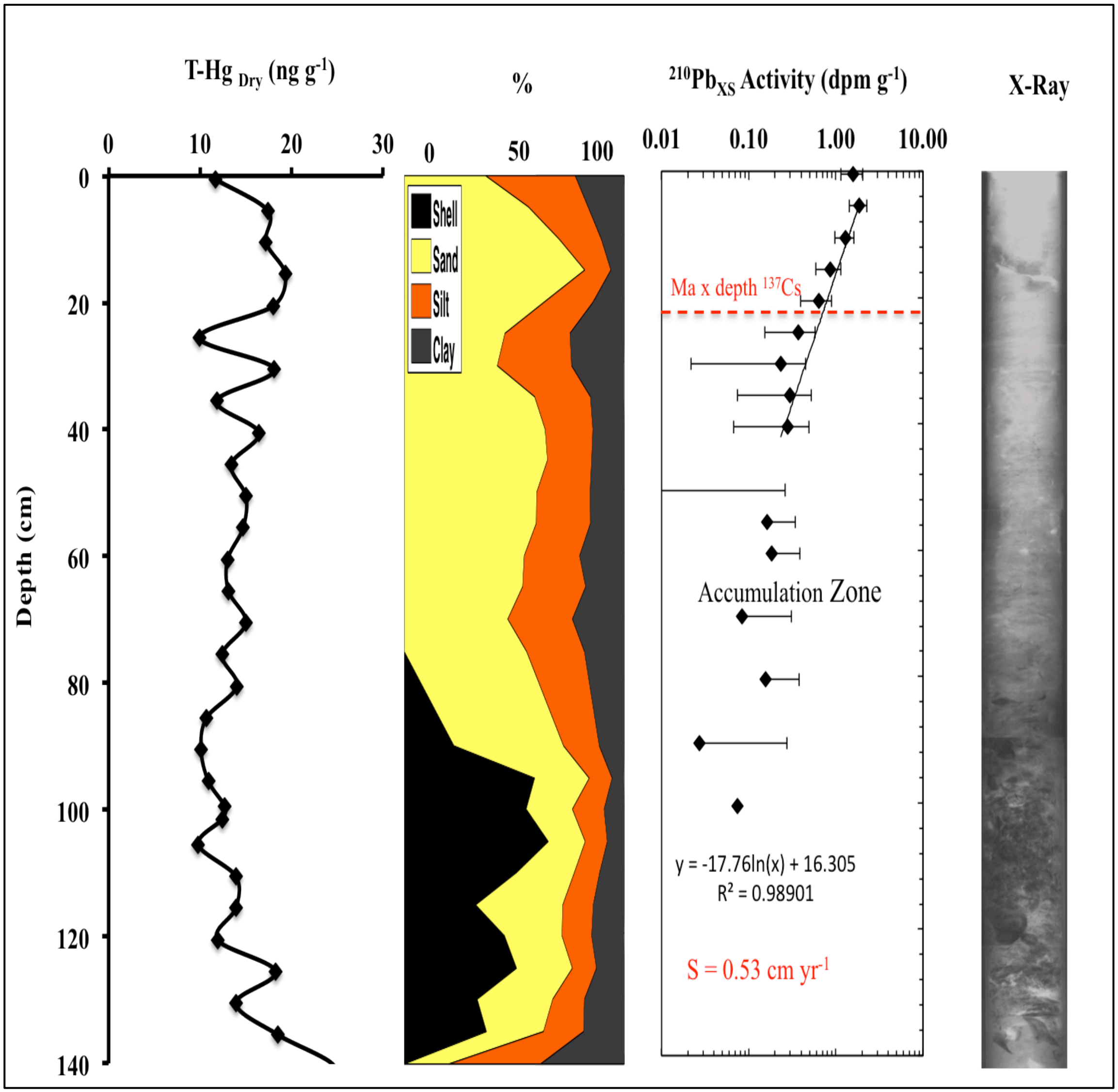

Figure 7. Vertical profile of total Hg concentration, grain size distribution, excess ^{210}Pb activity and X-ray for core collected in East Galveston Bay.

The background concentration of Hg in this location (figure 7) could not be determined due to the low concentration and as a results, the depth where Hg reaches it background values was not determined. The total Hg concentration is fluctuating between 10-20 ng g^{-1}, which is very low compared to other locations.

The grain size distribution profile shows that the sand fraction is between 40% and 60% for the upper 80 cm. There is an increase in shell content below 80 cm. The silt and clay fraction were about 50% for the upper 5cm, and decreases to a relatively constant value of about 20% throughout the remainder of the core. The coring site is in a back-bay environment proximal to a large washover fan along the northern shore of Bolivar Peninsula.

The excess ^{210}Pb profile contains a mixed layer for the upper 4 cm, below which the activity of ^{210}Pb decreases logarithmically with depth from 5cm to 30cm. the sediment accumulation rate of 0.53 cm yr^{-1} was calculated between these to points. The x-radiograph did show clear layering for the upper 30 cm. The maximum activity of 137Cs was at depth of 30 cm, and based on this the sediment accumulation calculated was 0.58 cm yr^{-1}. The land subsidence rate was estimated in this location to be 0.3 cm yr^{-1}.

3.3 Core 9 – Trinity Bay

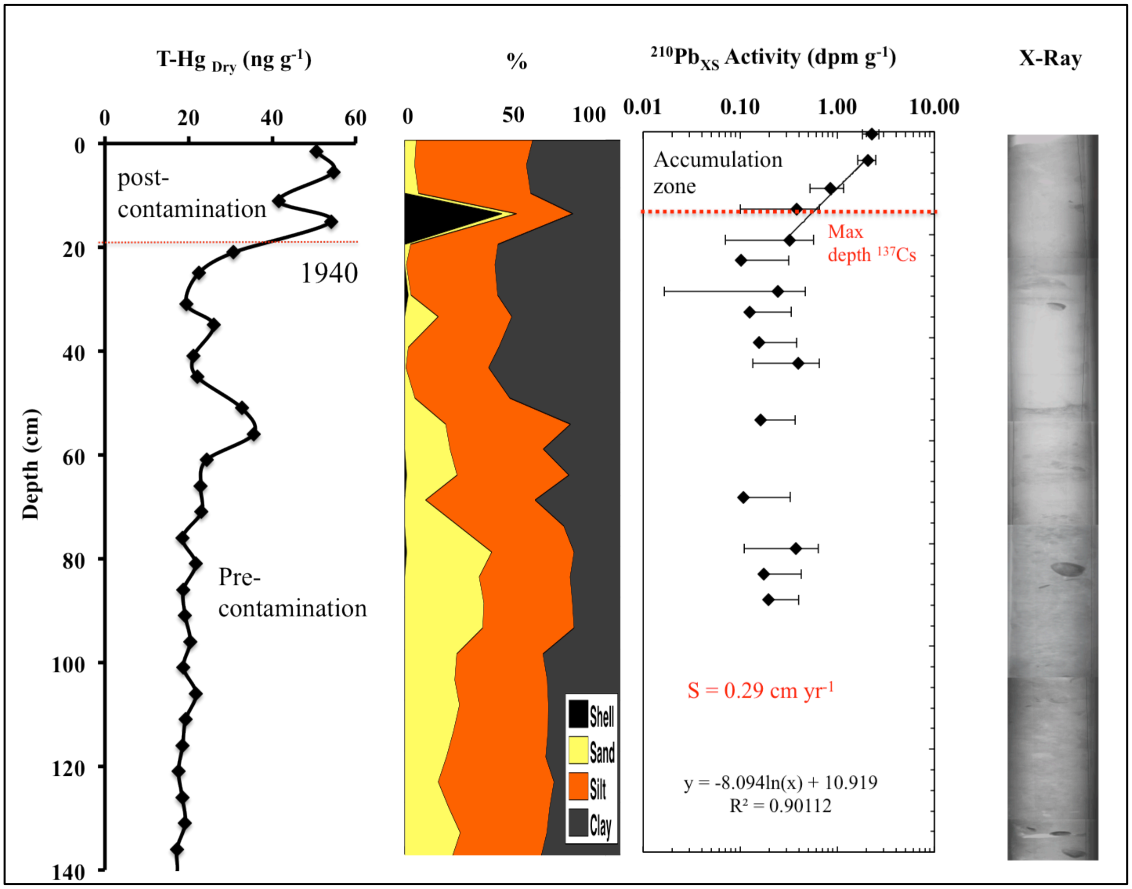

Figure 8. Vertical profile of total Hg concentration, grain size distribution, excess ^{210}Pb activity and X-ray for core collected in Trinity Bay.

Surface Hg concentration in Trinity Bay (figure 8) is 52.55 ng g^{-1} and decreases with depth. The background concentration of Hg was reached at depth 21cm. Hg concentrations ranged between 20 and 54 ng g^{-1}. A chronological horizon was determined based on the depth where Hg reaches background values as pre-contamination prior to 1940 the year when most industries were established.

The upper 40 cm of the grain size distribution profile is dominated by the silt and clay fraction, with less than 10% of sand. Between 15 and 20 cm there was some shells. Below a depth 45 cm, the sand fraction increases down the profile with an associated decrease in silt and clay fractions.

Between the periods of 1906-2000, the area experiences a land subsidence of 0.47 cm yr^{-1}. The sediment accumulation rate was 0.29 cm yr^{-1} calculated using ^{210}Pb based, on the decrease of activity between depth 5 and 55 cm. The maximum depth of ^{137}Cs activity was at 15cm, which indicate a sediment accumulation of 0.28 cm yr^{-1}.

3.4 Core 11 – Mid- Galveston Bay

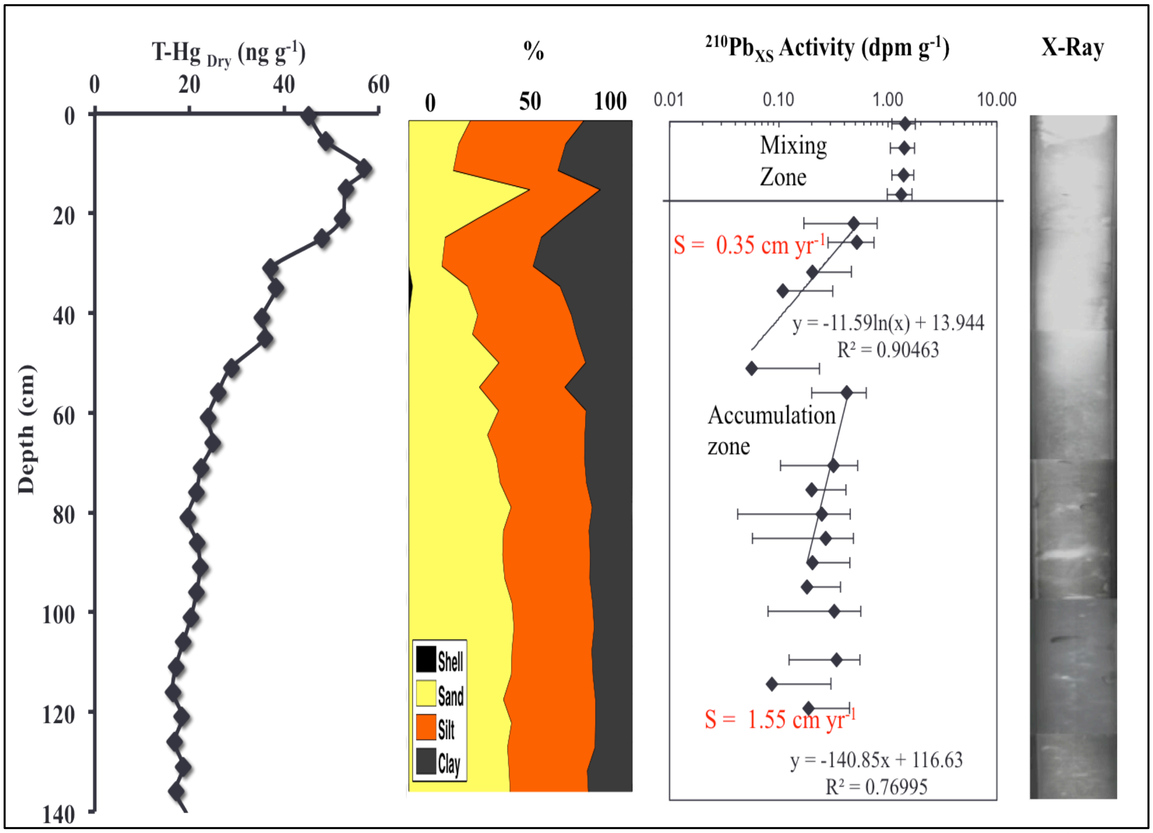

Figure 9. Vertical profile of total Hg concentration, grain size distribution, excess ^{210}Pb activity and X-ray for core collected in Mid-Galveston Bay.

Core 11 (figure 9) has an increase in Hg concentration from the depth where background values were found (116cm) to the top of the core. The average Hg concentration at the surface is 47 ng g^{-1}. The grain size distribution profile sand content of about 30% for the upper 30 cm below which the sand fraction increases to about 50%.

Land subsidence rate in this location is about 1.6 cm yr^{-1} with a two different sediment accumulation rates of 0.35 and 1.55 cm yr^{-1} obtained from ^{210}Pb. The excess ^{210}Pb profile shows a mixed layer for the upper 15 cm, with a relatively uniform activity between 1.3-1.4 dpm g^{-1} and two different intervals where the activity decreases logarithmically with depth that reflect the rapid increase in land subsidence in this area. The X-radiograph indicates that a combination of physical mixing and bioturbation in the upper 15 cm of the core. The depth of maximum activity of ^{137}Cs was at depth 171 cm (not shown in the profile), yielding a sediment accumulation rate calculated of 3.3 cm yr^{-1}.

3.5 Core 13 – Clear Lake

Total Hg concentration in Clear Lake (figure 10) fluctuating between 40 and 60 ng g^{-1} with the highest concentration of 61.4 ng g^{-1}. At depth 95.5, Hg reaches its background value where the concentration is constant with depth. The boundary between pre and post contamination is easily determined and the year were Hg starts to increase is assumed to be 1940. The grain size distribution profile shows low sand fraction for the upper 60 cm, below which it increases with depth where silt and clay fraction decrease to about 50%.

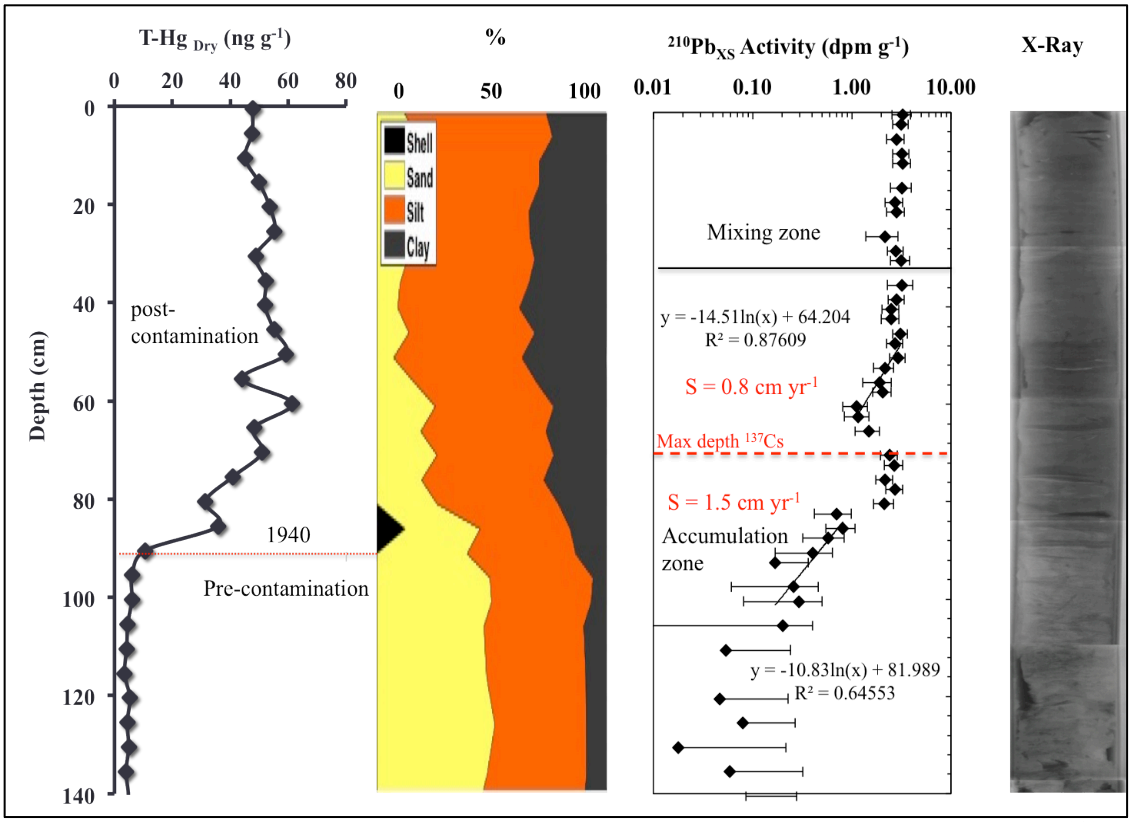

Figure 10. Vertical profile of total Hg concentration, grain size distribution, excess ^{210}Pb activity and X-ray for core collected in Clear Lake.

Clear Lake has experience a land subsidence rate of about 1.8 cm yr^{-1} between the periods of 1906 and 2000. The profile of excess ^{210}Pb shows a mixed layer in the upper 30 cm, with a uniform activity and decreases logarithmically with depth below 30 cm. Two sediment accumulation rates were calculated based on the decreasing of the ^{210}Pb activity between 21-28 cm and 35-42 cm of 0.8 and 1.5 respectively. The maximum depth of ^{137}Cs activity was at 67 cm, which indicate a sediment accumulation of 1.068 cm yr^{-1}.

3.6 Core 15 – Taylor Lake

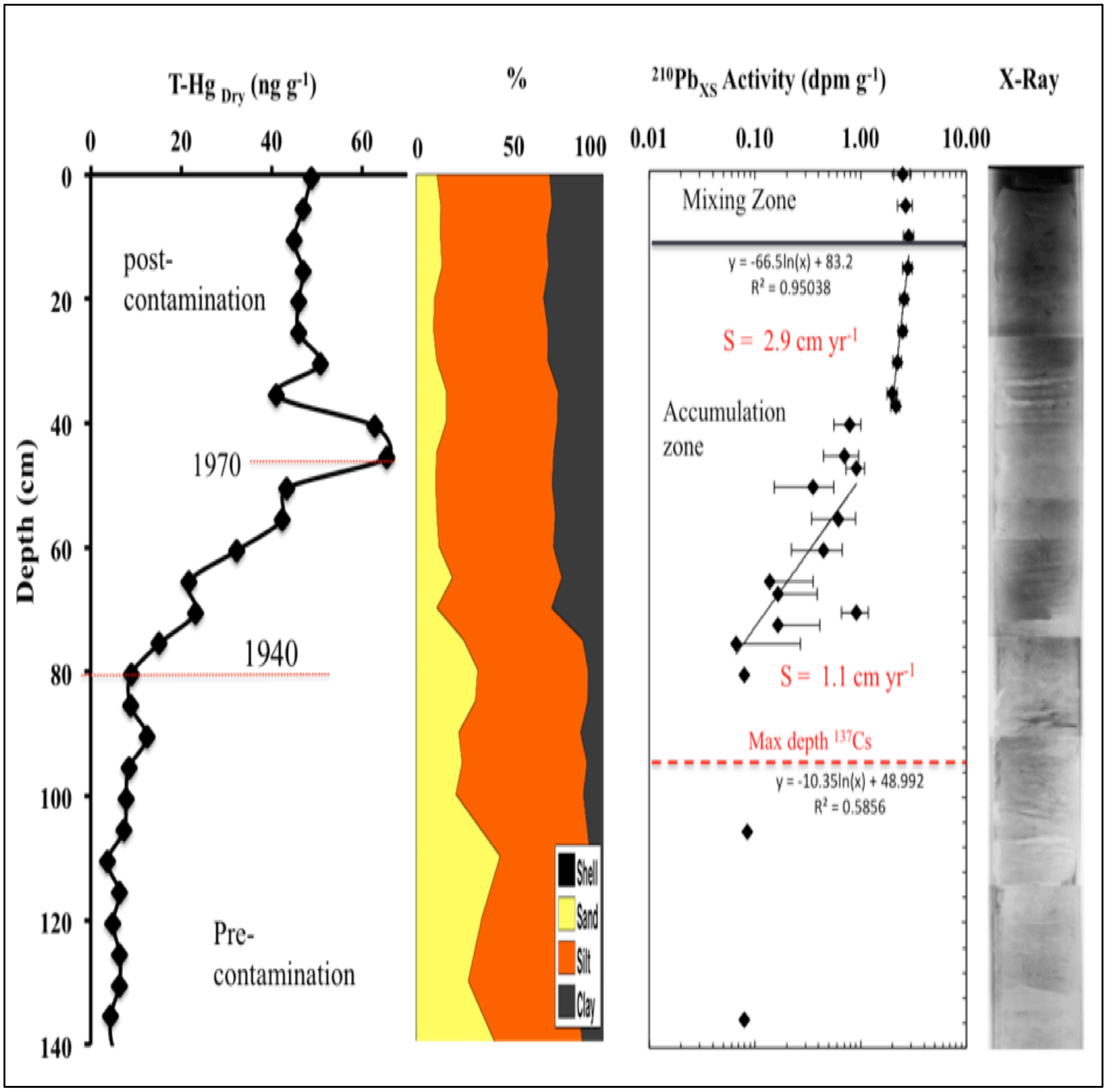

Figure 11. Vertical profile of total Hg concentration, grain size distribution, excess ^{210}Pb activity and X-ray for core collected in Taylor Lake.

The total mercury concentration profile obtained from core 15 (figure 11), from Taylor Lake, shows Hg concentrations fluctuating between 4 and 60 ng g^{-1} and concentrations decrease with depth. There is a pronounced peak in Hg concentration at depth 45.5 with the highest value of 65.5 ng g^{-1}. At depth 80.5 cm, Hg concentration reaches the background value of about 4 ng g^{-1}. The average surface Hg concentration for the upper 5 cm is 47.6 ng g^{-1}.

As with Core 13 from Clear Lake, the grain size distribution profile shows low sand fraction for the upper 60 cm below which the sand fraction increases with depth to 27%

Land subsidence rate in Taylor Lake is estimated to be 1.87 cm yr^{-1} between the period of 1906 and 2000. The profile of excess ^{210}Pb shows a mixed layer in the upper 10 cm, with a consistently activity and decrease logarithmically with depth. The X-radiograph shows a combination of physical laminations and burrowing suggesting that mixed layer results from a combination of physical mixing and bioturbation. Two sediment accumulation rates were calculated based on the decreasing of the ^{210}Pb activity of 1.1 and 2.9 respectively based on the decreasing of the ^{210}Pb activity. The maximum depth of ^{137}Cs activity was at 95 cm, which indicate a sediment accumulation of 2.55 cm yr^{-1}. Based on the ^{210}Pb chronology the year where Hg reaches it peak is about 1972.

3.7 Core 18 – Upper Galveston Bay

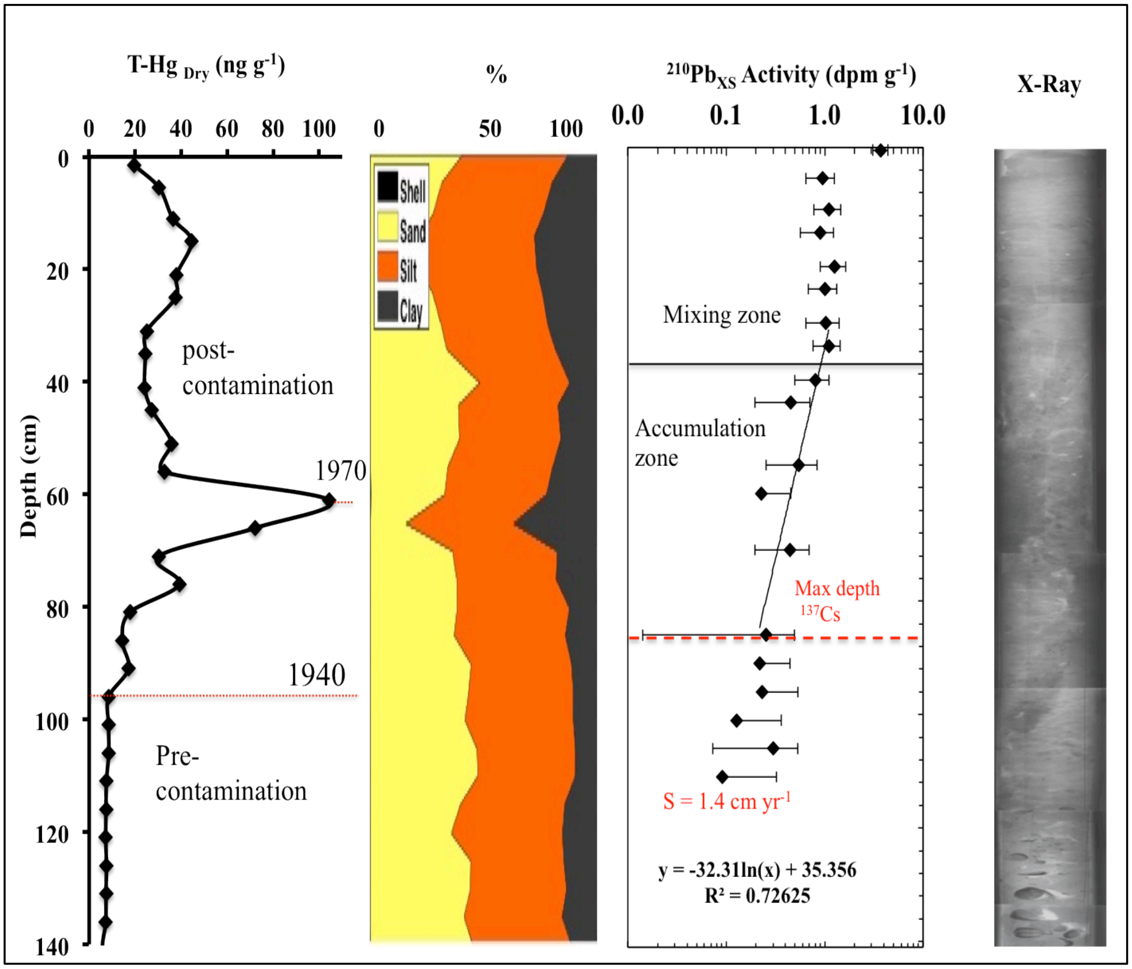

Figure 12. Vertical profile of total Hg concentration, grain size distribution, excess ^{210}Pb activity and X-ray for core collected in Upper Galveston Bay.

The total Hg profile was constant with depth for the upper 55 cm with values ranging between 20 and 40 ng g^{-1} (figure 12). A pronounced peak of Hg concentration with a value of 104.3 ng g-1 exists a at depth of 61 cm. At a depth of 96 cm Hg reaches the background value of 7 ng g^{-1}. This Hg profile generally shows an upward increase in concentration. The sand, silt, and clay fraction in this core are nearly uniform throughout the core with about 40% sand, 40 %silts, and 20% clay.

Excess ^{210}Pb profile contains a mixed layer for the upper 40 cm of the core, with activity ranging between 0.9 and 1.1 dpm g^{-1}, and the activity decreases logarithmically with depth below the mixed layer. A sediment accumulation rate obtained from ^{210}Pb is 1.4 cm yr^{-1}. This region has a land subsidence rate of about 1.9 cm yr^{-1}. The maximum depth of ^{137}Cs activity was at 86 cm, which indicate a sediment accumulation of 0.7 cm yr^{-1}.

3.8 Core 20 – Tabbs Bay

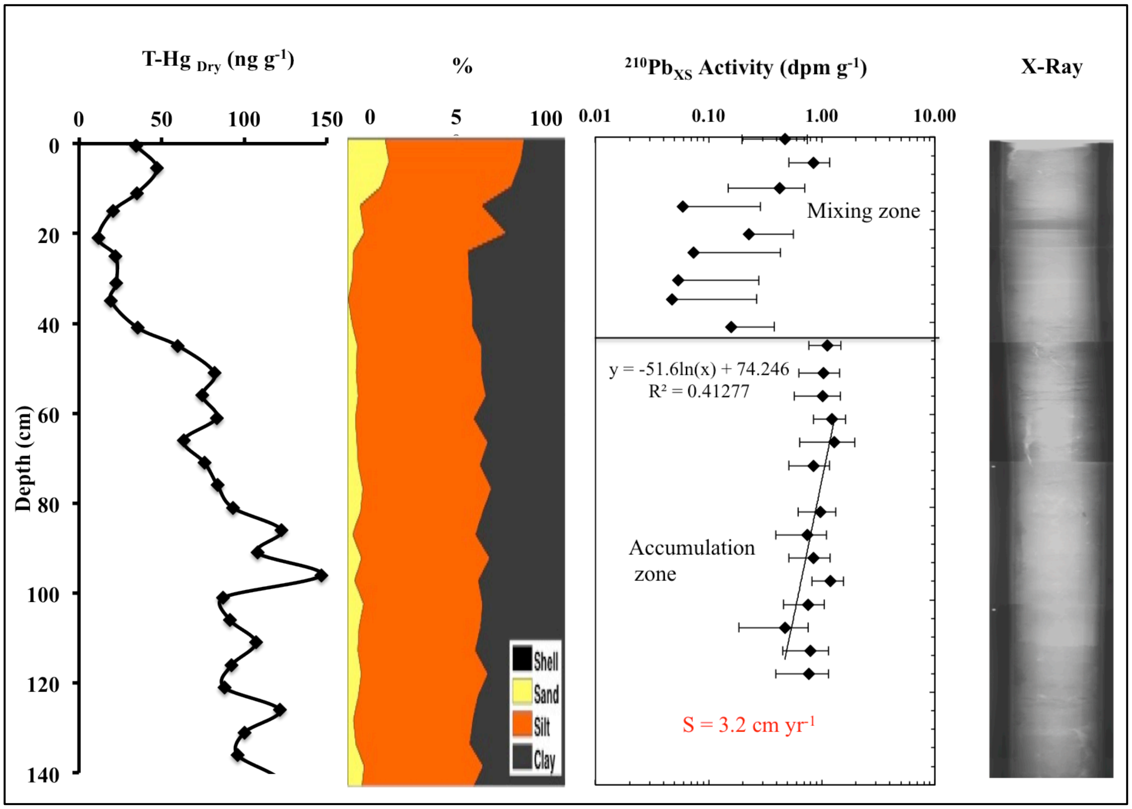

Figure 13. Vertical profile of total Hg concentration, grain size distribution, excess ^{210}Pb activity and X-ray for core collected in Tabbs Bay,SJR/HSC.

At this location (figure 13), Hg concentrations fluctuate between 21 and 146 ng g^{-1}. Surface Hg concentration for the upper 5 cm was 48.85 ng g^{-1}, below which the concentration increases with depth to a maximum value of 146 ng g^{-1} at depth of 96 cm. In order to reach the background depth, a deeper core is required. Consequently, the Hg and radioisotope profiles are incomplete. In general, the grain size distribution shows that the most dominant fraction in this location are the silt and clay, with a sand fraction of 10%.

The excess ^{210}Pb profile shows two distinct layers. Although the activity decreases logarithmically in the upper zone, it is assumed to be the mixing zone because of the location of this core near the dredged channel and the upper portion of the profile is interpreted to result from older sediment sitting atop younger sediment. The sediment accumulation rate was calculated to be 3.2 cm yr^{-1}. In this region, land subsidence rate is about 2.9 cm yr^{-1} between the periods of 1906 -2000.

3.9 Core 22 – Scott Bay

This core (figure 14) contains the highest Hg concentration found in any core from this study. The average Hg concentration at the surface is 157.85 ng g^{-1} with a maximum value of 2374.4 ng g^{-1} at 76 cm depth. The concentration remains roughly uniform from the surface to about 60 cm below which it increases to its peak below which it decrease with depth to where it reaches the background value at depth 131 cm.

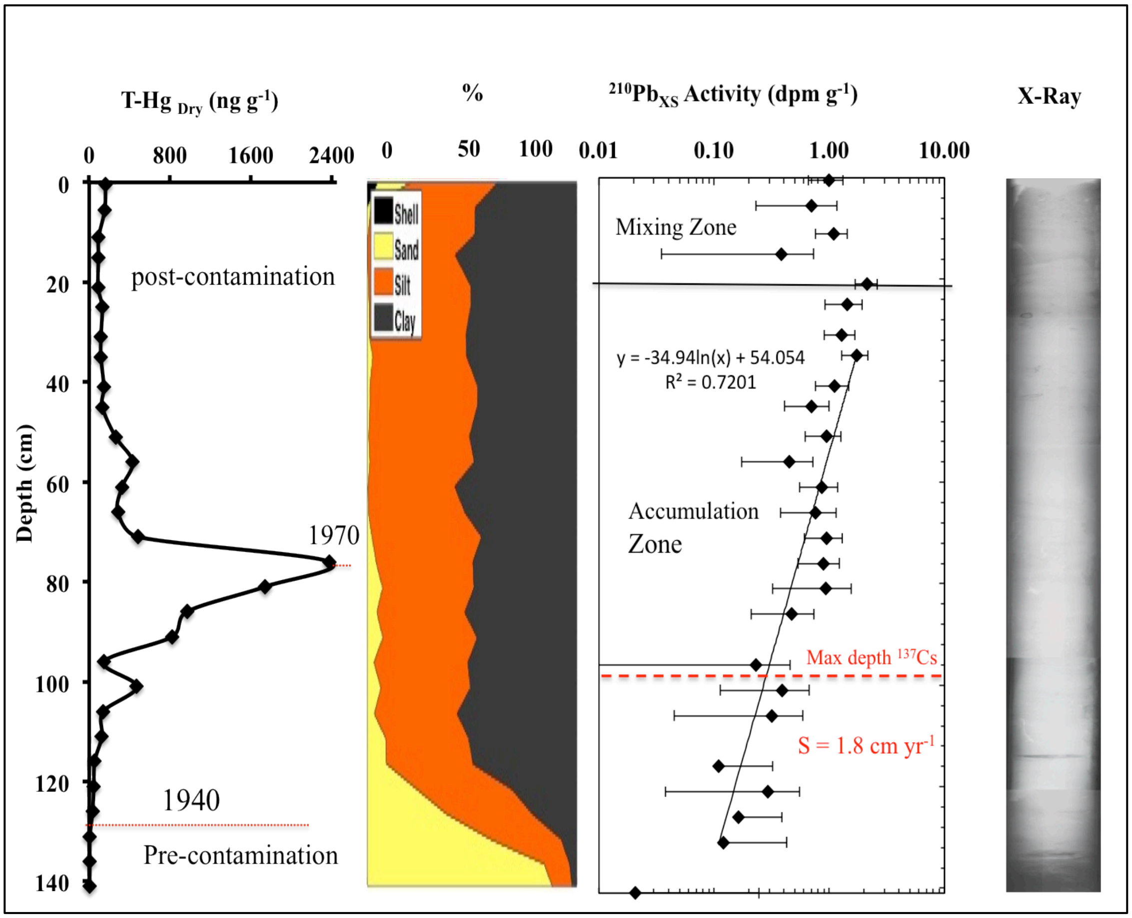

Figure 14. Vertical profile of total Hg concentration, grain size distribution, excess ^{210}Pb activity and X-ray for core collected in Scott Bay, SJR/HSC.

The grain size distribution profile shows that the most dominate fraction for the upper 120 cm is silt and clay, with less than 5% of sand. At depth 120, the sand content increases to about 90%. In this location the land subsidence rate is 2.4 cm yr^{-1} between the periods of 1906 -2000.

The excess ^{210}Pb profile contains a 20 cm deep mixed layer in the upper core and activities logarithmically with depth. The sediment accumulation rate obtained using ^{210}Pb is 1.8 cm yr^{-1}. The maximum depth of ^{137}Cs activity was at 100 cm, which indicate a sediment accumulation of 1.6 cm yr^{-1}.

4. DISCUSSION

4.1 Land subsidence / Sedimentation rate

The historical data obtained from USGS and HGSD documenting land subsidence rates for the last 100 year were correlated with the calculated sediment accumulation rates obtained from ^{210}Pb and ^{137}Cs to determine whether sedimentation kept pace with land subsidence. Sediment accumulation rates calculated from ^{210}Pb (figure 15) show a gradient of accumulation throughout the bay with higher sediment accumulation rates in SJR/HSC and rates deceasing both down the salinity gradient of the bay as well as away from the center of highest land subsidence.

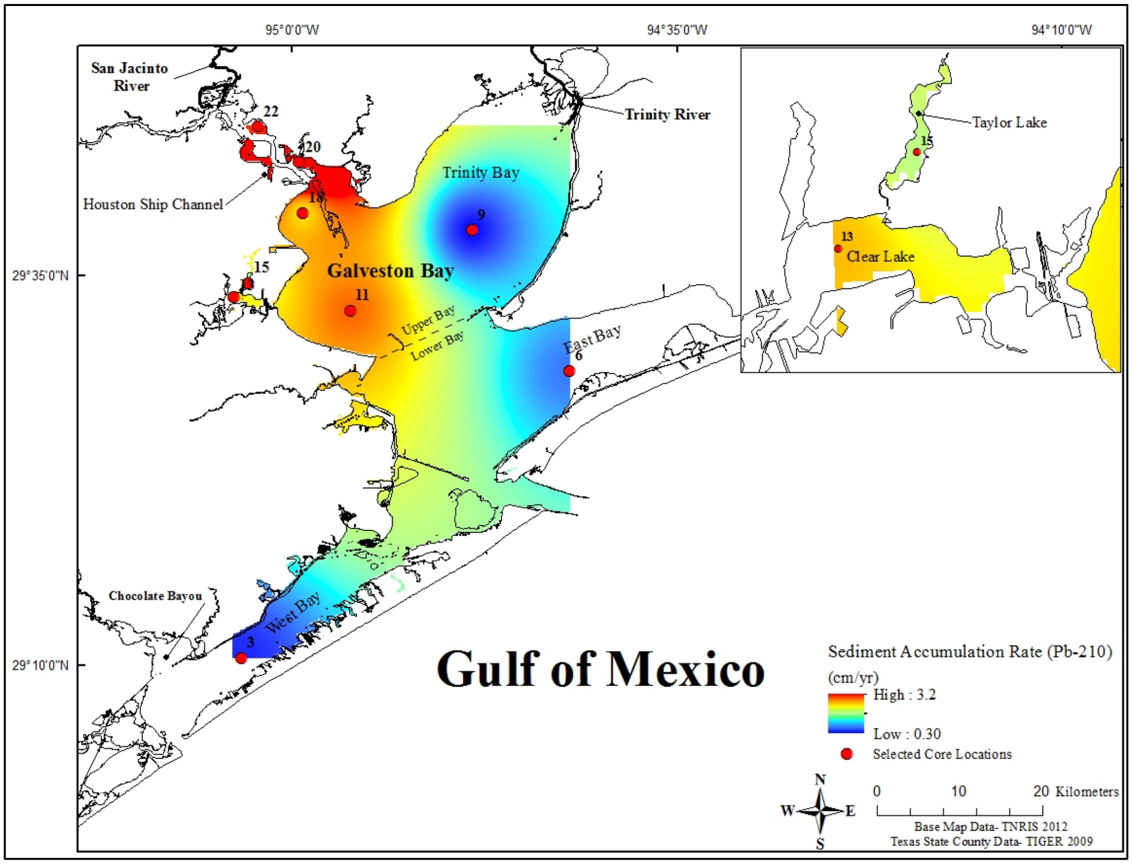

Figure 15. Areal distribution of the sediment accumulation rate calculated using ^{210}Pb.

Sediment accumulation rates for Cores 22 and 20 in SJR/HSC (1.8 and 3.2 cm yr^{-1} respectively) are comparable to previous calculation of 2.58 cm yr^{-1} [*Yeager et al*, 2007]. The land subsidence rate in this region is estimated to be between 2.4 and 2.9 cm yr^{-1}. Additionally, Core 18 has a sediment accumulation rate of 1.4 cm yr^{-1}, which is also consistent with *Yeager et al*, 2007. The land subsidence rate at this site is 1.9 cm yr^{-1}. Sediment accumulation rate for Core 9 in Trinity Bay is 0.29 cm yr^{-1}, which is comparable to previously published rates of 0.29 cm yr^{-1}[*Santschi et al*, 2001] and 0.44 cm yr^{-1}[*Yuill*, 1991] for nearby cores. In addition, Cores 3 and 6 shows sediment accumulation rate of 0.34 and 0.53 cm yr^{-1} with a land subsidence rate of 0.3 and 0.46 respectively.

The ^{210}Pb transection A-A' (figure 16) shows sediment accumulation rate along the transect and the depth of the mixing zone. In general, there is a decrease in the accumulation rates away from the SJR/HSC towards the distal parts of the bay (e.g. Core 6), and areas with higher land subsidence rates have deeper mixing zones within the cores, such as Cores 20 and 18.

Table 2 shows the comparison between sedimentation rates to land subsidence rates. In addition to land subsidence rates, the rate of Global Sea Level Rise (GSLR) needs to be considered. Land subsidence was measured on land and is an independent measure to GSLR. According to US *EPA* (2010), between 1870 and 2008, the average GSLR rate has been 0.17 cm y^{-1}. The rate of the creation of accommodation space in the Galveston Bay system is going to be the sum of land subsidence and GSLR. Both rates are shown in Table 2. Although the general trend is that where subsidence rates are high sedimentation rates are high, there is not a perfect match with land subsidence. Differences between land subsidence and sedimentation rate range between +77% and -41%, with negative values representing sedimentation rates lower than subsidence rates. When adding an average GSLR rate, the differences are even greater, and range is between 11% and -121% and in fact, only in the Tabbs Bay,West Bay and Taylor Lake cores does it appear that sedimentation kept pace with RSLR, with a surplus of sedimentation of 4%, 11% and 30 respectively. Cores from Central Galveston Bay,

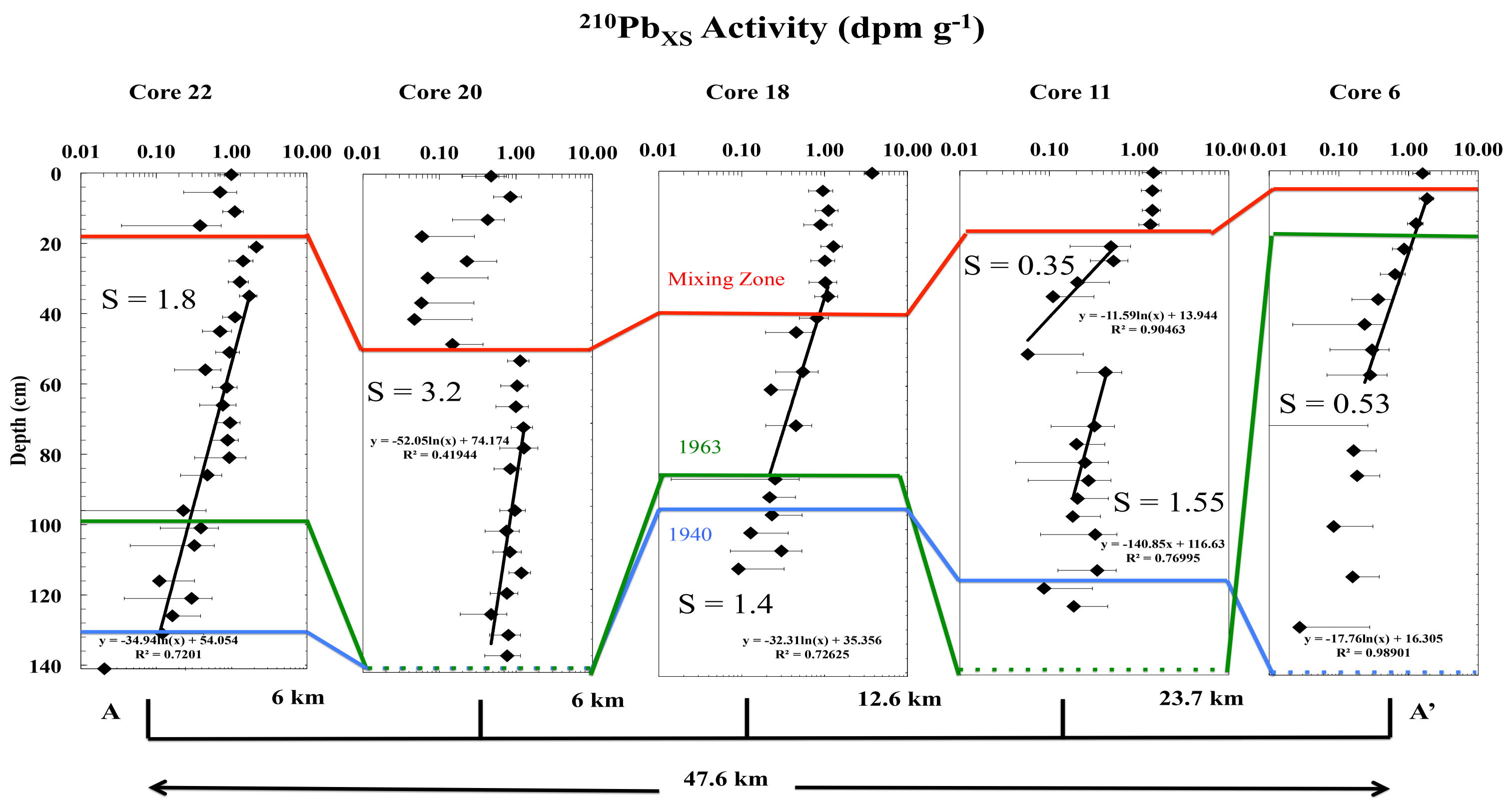

Figure 16. Cross-section of ^{210}Pb transect through core 22 to core 6 in Galveston Bay. The correlation based on radionuclide dating and the depth of background level of Hg. Transect location is shown in figure 1 (cross section A-A'). Sedimentation rate are shown within plot. The dashed line indicates that the correlation is missing or deeper in the core. Blue line indicates 1940s, green line indicates the maximum depth of ^{137}Cs in 1963, and red line indicates the mixing zone in each location. Distance between cores is indicated in km.

Clear Lake and East Galveston Bay had sedimentation rates ranging between -14 and -38% of subsidence and the other sites had sedimentation rates ranging from -48% to -121%.

Core 15 is from Taylor Lake is an example which sedimentation kept pace with RSLR. In 1944, Taylor Lake was a freshwater lake separated from Clear Lake by a creek and wetlands. Today, Taylor Lake is a small tidal lake extending to the north from Clear Lake and the tidal creek and wetlands have a dredged channel through them. Additionally, dredge and fill has created bulkheaded canal communities around nearly the entire shoreline of Taylor Lake and a significant portion of the drainage basin has been modified, resulting a highly altered system. These additional anthropogenic alterations likely significantly impacted sediment delivery to Taylor Lake and may well provide explanation for the sedimentation rate being 30% higher than the RSLR.

The outliers, where there was the greatest difference between subsidence and sedimentation are for Cores 9, 18 and 22. There are likely site-specific explanations for these differences.

Core 9 was collected in Trinity Bay and the land subsidence rates are calculated from land-based benchmarks mainly along the western shore of Galveston Bay. Core 9's location is 17 km from the north shore, 21 km from the western shore and 9 km from the eastern shore, likely at least 20 km from the nearest benchmark. The contours for subsidence in figure 4 are very wide in this area and based off of data at least 25 km from the coring location. Consequently, the land subsidence rate for this part of the bay is poorly constrained. It may well be that there is a much better agreement between sedimentation and subsidence in this area and that the difference presented here simply reflects a poorly constrained subsidence rate.

Core 18 is in upper Galveston Bay 1.3 km west of the portion of the Houston Ship Channel that extends through the open portion of Galveston Bay. Along this section, the dredge spoils are piled to the east of the channel so there is nothing dissipating tanker wakes to the west. Personal communications with the U.S. Army Corps of Engineers revealed that sediment dynamics in this area are very complex, mainly driving by the bow wakes of tankers, which has causes scouring of the bay bottom to the west of the channel, in the Core 18 location and convergence of sediment within the ship channel, requiring nearly continual dredging of the channel. This enhanced scouring likely explains the 26% deficit in sediment accumulation when compared to subsidence.

Core 22 in Scott Bay is in the middle of the heart of the petrochemical industry along the SJR/HCS as well as being situated within the area where there was maximum subsidence and is directly adjacent to the HSC. Since 1944, there has been significant loss in wetland and saltmarshes (figure 17). These factors likely all contribute a sediment deficit at this location and likely explain why sediment accumulation rate is 43% lower than relative sea level rise.

1944 1953 1978 2012

Figure 17. Loss in wetland and saltmarshes in Scott Bay since 1944 [*Google Earth,* 2013]

4.2 Spatial and temporal distribution of total Hg in Galveston Bay

The total Hg concentration for the upper 5 cm in Galveston Bay ranged between 14.5 and 157.8 ng g^{-1} with an average of 50 ng g^{-1} (Table 1). The spatial distribution of Hg in the bay was found to be dramatically higher in areas around SJR/HSC and decreasing seaward (figure 18). In general, Hg concentration in the lower bay is lower than the upper bay and within the background range. However, the concentration of Hg in SJR/HSC is much higher due to the proximity to most of the petrochemical plants and the Chlor Alkali plant.

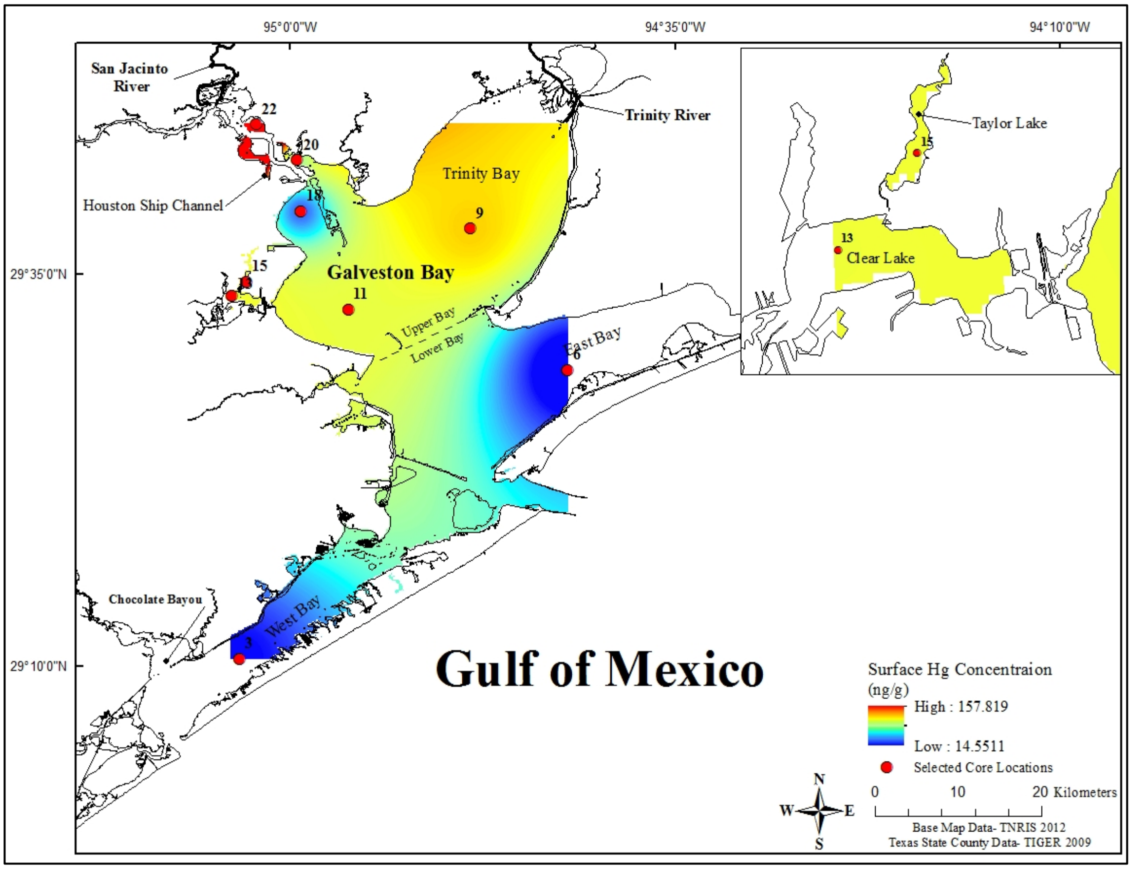

Figure 18. Areal distribution of the average surface Hg concentration for the upper 5 cm of each core in Galveston Bay.

Figure 19 represent the maximum concentration of Hg in each core. Core 22 has the maximum concentration among all of the cores with a value of 2374.4 ng g^{-1}, the maximum concentration in Core 20 and 18 was 146 and 104 respectively (Table 1). The maximum concentration decreases dramatically towards GOM, indicating that most Hg has been preserved in the upper portion of the bay where sediment accumulation and land subsidence are highest.

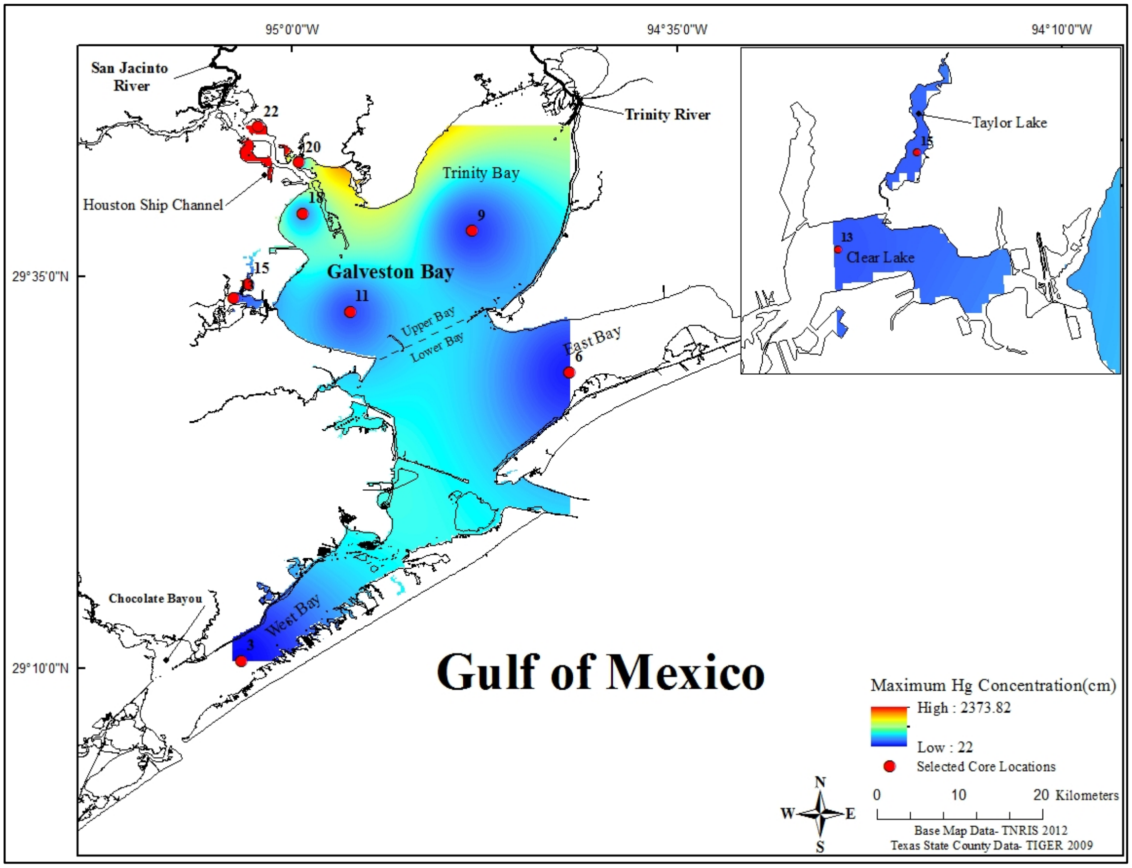

Figure 19. Areal distribution of the maximum Hg concentration in each core in Galveston Bay.

The depth where anthropogenic Hg concentration reaches its maximum values varies in each core (figure 20). Core 3 and 6 shows a value of zero, which means that the depth of the anthropogenic Hg concentration could not determined due to the low concentration in these locations compare to the other locations. The depth of this concentration were highest in Cores 20 and 22. This observation supports the idea that in these locations it is high sediment accumulation rate and higher land subsidence that causes Hg concentration to be store deeper in the sediment column.

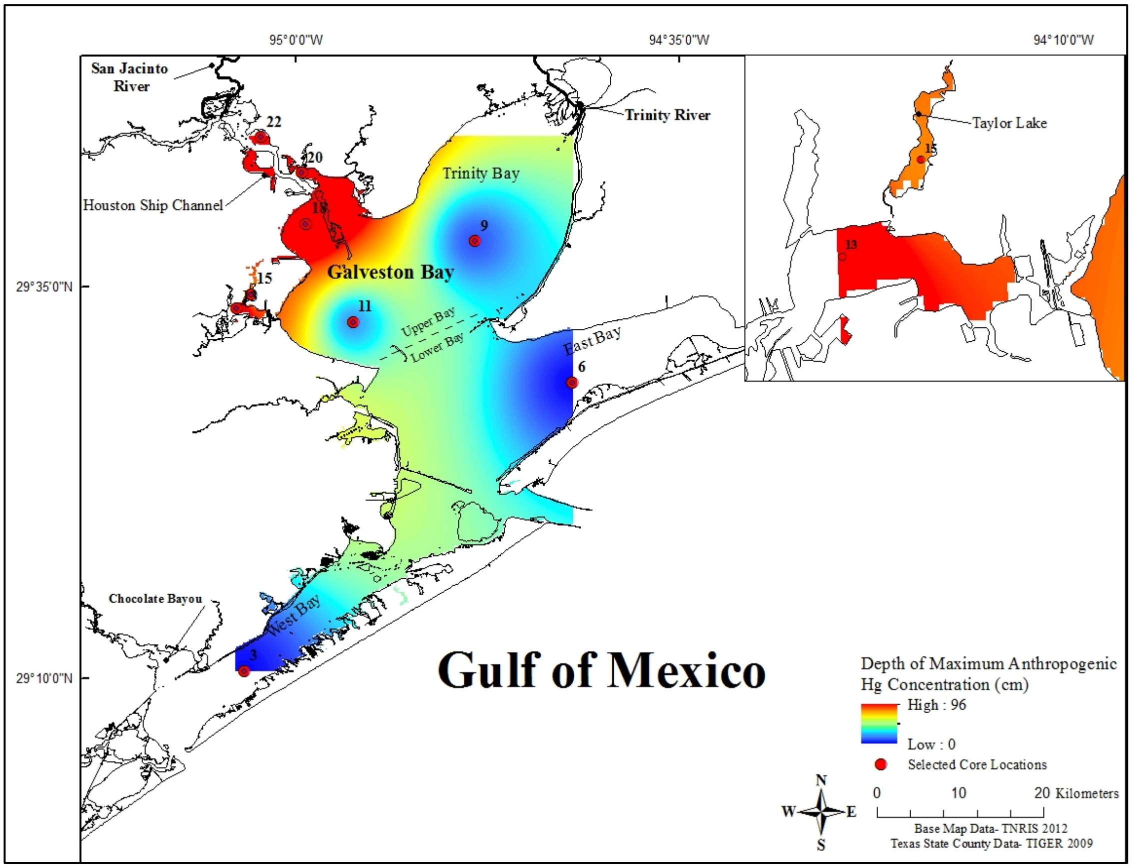

Figure 20. Areal distribution of the depth of maximum anthropogenic Hg concentration of each core in Galveston Bay.

Additionally, the depth of the background values of Hg varies as well (figure 21), being deeper in SJR/HSC and shallower toward the GOM. Cores 3, 6 and 20 has the depth of the background values at zero, which means that the background depth could be

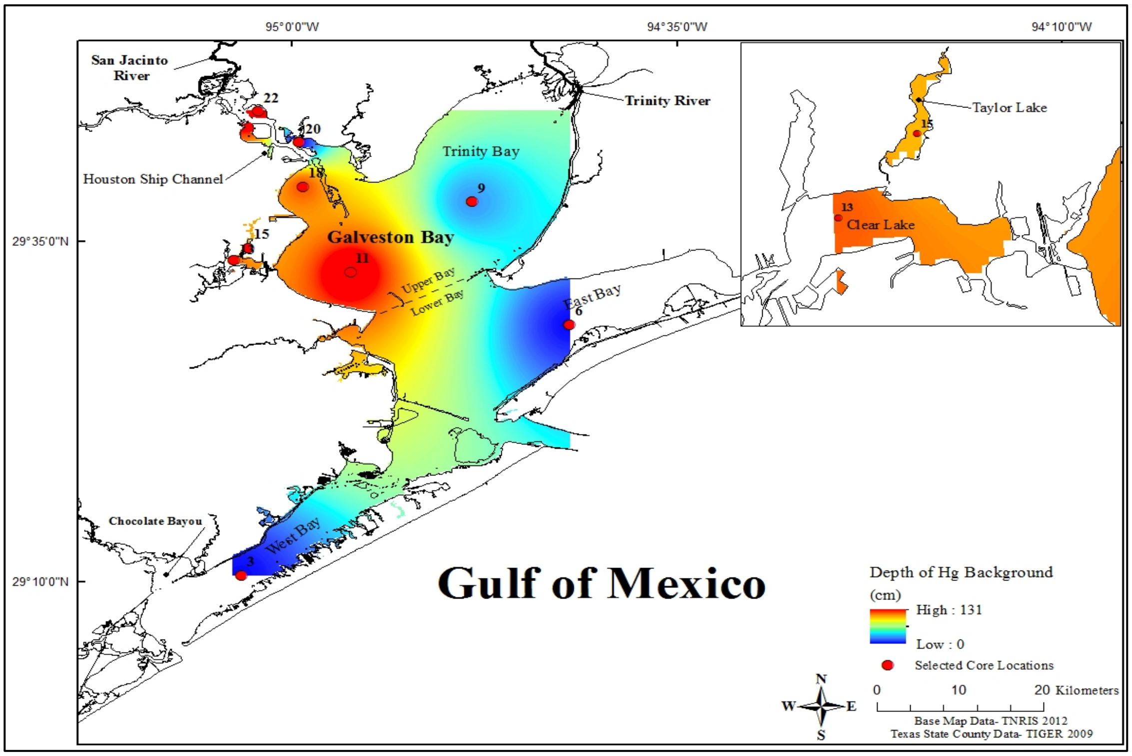

Figure 21. Areal distribution of the depth Hg concentration background of each core in Galveston Bay.

determined because either there is low concentration in Hg or the core is not deep enough to detect the background depth, as is the case for Core 20. The depth where Hg reaches it is background value can be used as a proxy in order to determine sediment accumulation rate and the temporal changes in the bay. A shallower background will indicate a low sediment accumulation rate, which reflect the system has not received a high input of Hg over many years.

In general, Hg concentration at the surface sediment in most locations are within 2 to 3 factors higher than the background values or even more comparable to Core 20 and 22. There is a significant portion of anthropogenic input of Hg being accumulated in areas proximal to SJR/HSC, which indicate that this area is a suitable place to store Hg in the sediment as a result of the higher input and higher sediment accumulation rate along with land subsidence.

^{210}Pb and ^{137}Cs were used to reconstruct the historical input of Hg in Galveston Bay (figure 22). In most cores, the increase in Hg concentration above background concentrations occur approximately around 1940, with a clear peak around 1970, and then a dramatic decrease in concentration to the surface. Hg in Galveston Bay was introduced to the system mainly due to the activities associated with the chlor-alkali plant, which began operation in 1948 [*ChemPlants*, 2013]. Another possible source is the atmospheric Hg input from refineries in the region.

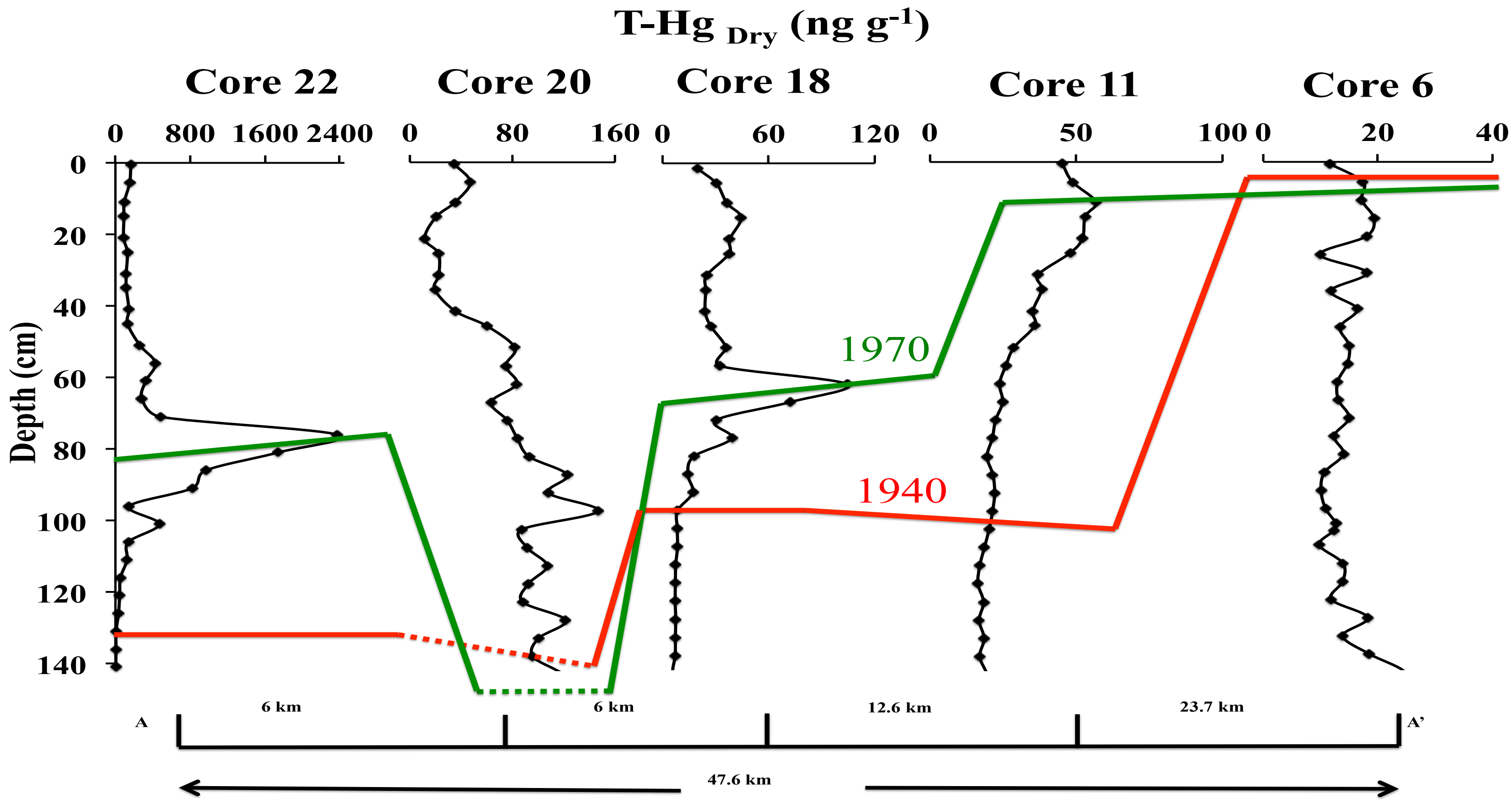

Figure 22. Cross-section through core 22 to core 6 in Galveston Bay. The correlation based on radionuclide dating and the depth of background level of Hg. Transect location is shown in figure 1 (cross section A-A'). The dashed line indicates that the correlation is missing or deeper in the core. Red line indicates 1940s and green line 1970s. Distance between cores is indicated in km.

4.3 Hg as a geochronology tool

The Hg concentration profile has been use as a geochronology tool to determine sediment accumulation rate for specific regions where there is clear anthropogenic loading of Hg. Hg profiles consequently shows how the load of Hg to the sediment have changed with time [*Louchouarn and Lucotte*, 1998]. In 1980, *Barbeau et al*, indicate that Hg can be used as a core dating method similar to ^{137}Cs isotopes in the Saguenay Fjord.

The mercury concentration profile from each core where there is distinguishable elevated concentrations is compared to the radioisotope geochronologies. It is assumed that the depth where mercury concentration started to increase is the depth at which the time of anthropogenic activities started in the bay (~1940). In general, sediment accumulation rates obtained using Hg profile are in good agreement with ^{210}Pb and ^{137}Cs results (table 2 and 3). Sediment accumulation rates for Cores 3, 6 and 20 could not be determined because it is difficult to distinguish the depth where Hg input started to increase or the concentration are within the background values. Moreover, Cores 18 and 22 show a discrepancy between sediment accumulation rate obtained from Hg and radioisotopes, which might be due to the bioturbation, in combination with land subsidence, which affect the depth where Hg background is reached

Table 3. Sediment accumulation rate obtained using Hg

	Core 3	Core 6	Core 9	Core 11	Core 13	Core 15	Core 18	Core 20	Core 22
Hg S_{Avg}	N/A	N/A	0.3	N/A	1.5	2.9	0.9	N/A	1.5

Thus, sediment accumulation rate and geochronology in Galveston Bay can be determined by using total Hg concentration and radioisotopes with the assumption that 1940 is the year where most industries were established, but is best used in conjunction with other geochronology tools such as ^{210}Pb and ^{137}Cs.

4.4 Hg and grain size fraction

Ding et al (2009) mentioned that Hg concentration is well correlated with organic matters OM, pH, silt and clay fractions and mercury was not well correlated with sand fractions. On the other hand, *Windom et al* (1989) said that there is no correlation between concentration of mercury and aluminum (an indicator of clay minerals) in marine sediments. This is because most of the labile mercury in sediment is complexed with particulate and dissolved organic matter in the sediments and not with clay particles or iron oxide coating on clay particles. Hg is mostly associated with organic matter, which will tend to be associated with fine particulates. Hg is associate with clay but in fact, it is because it tends to be associate with the OM that is sorbed onto fine particles (clays). Al (as in aluminosilicates) concentrations do not necessarily correlate well with Hg concentrations (if the clays do not contain much OM). Sand, and other coarse grained sediments generally are depleted in OM and thus generally do not much Hg associated with them.. The sulfur-containing functional group is the reason for this strong interaction between Hg and OM. The surface to volume ration and the chemical composition within the clay-sized fraction tend to bind large amounts of Hg (*Acquavita et al*, 2012). The relationship between Hg concentration and grain size fraction was examined for the 9 cores. In general, Hg concentration is well correlated with silt and clay fractions. On the other hand, the sand fraction is not well correlated with Hg. Corrolations between grain size and Hg concentration for some coring locations are shown in Appendix B. In Core 13, for example, Hg is well correlated with clay fraction (r = 0.86) and silt fraction (r = 0.67). However, with the sand fraction it was negatively correlated (r = 0.88) (figure 23). Transect A-A' (figure 24) reveal that a high amount of fine-grained sediment is accumulating in areas around SJR/HSC and are coarser seaward, which also supports the idea that Hg is associated with fine-grained sediment.

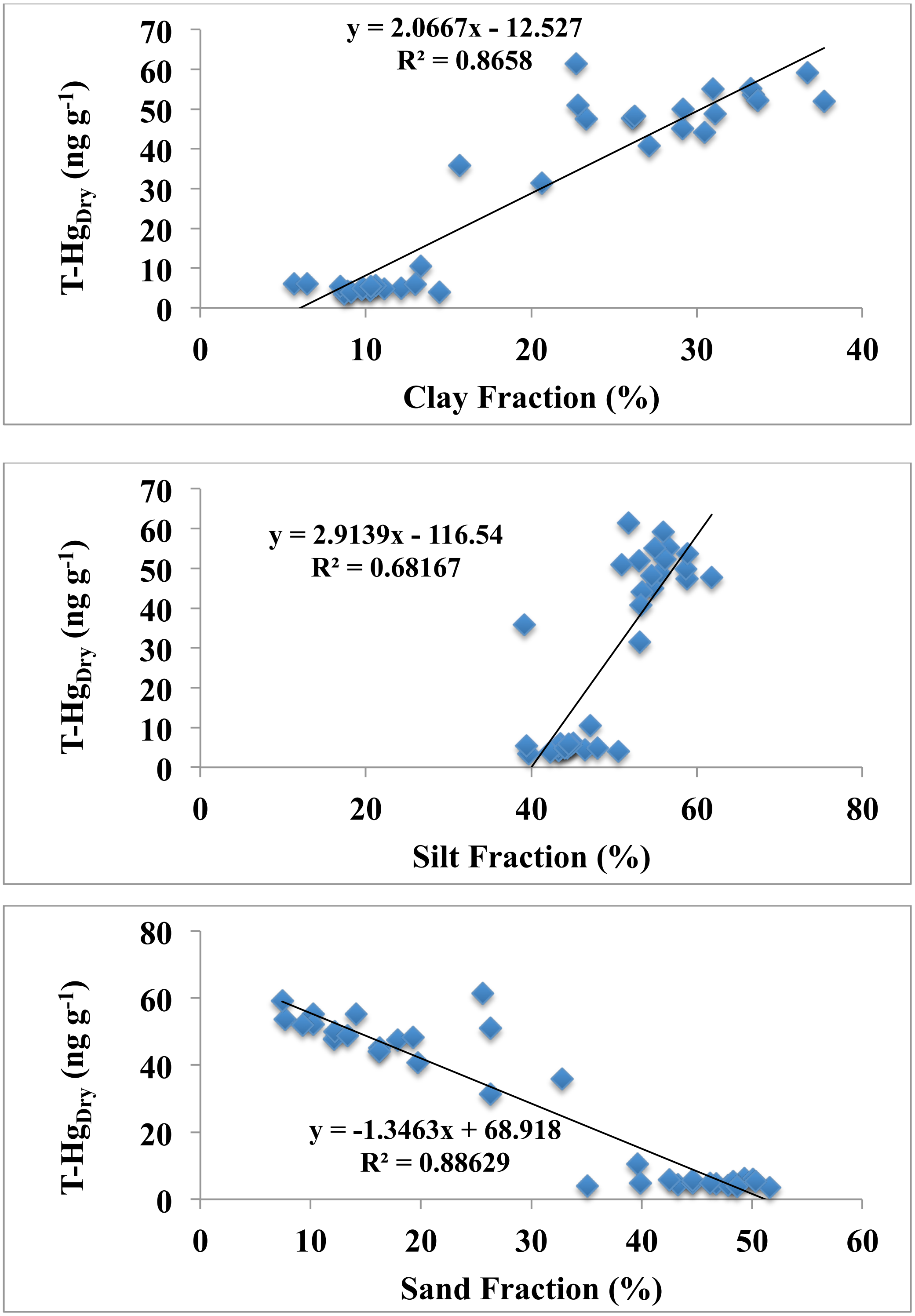

Figure 23. Correlation between Hg concentration and the percentage of grain size fraction

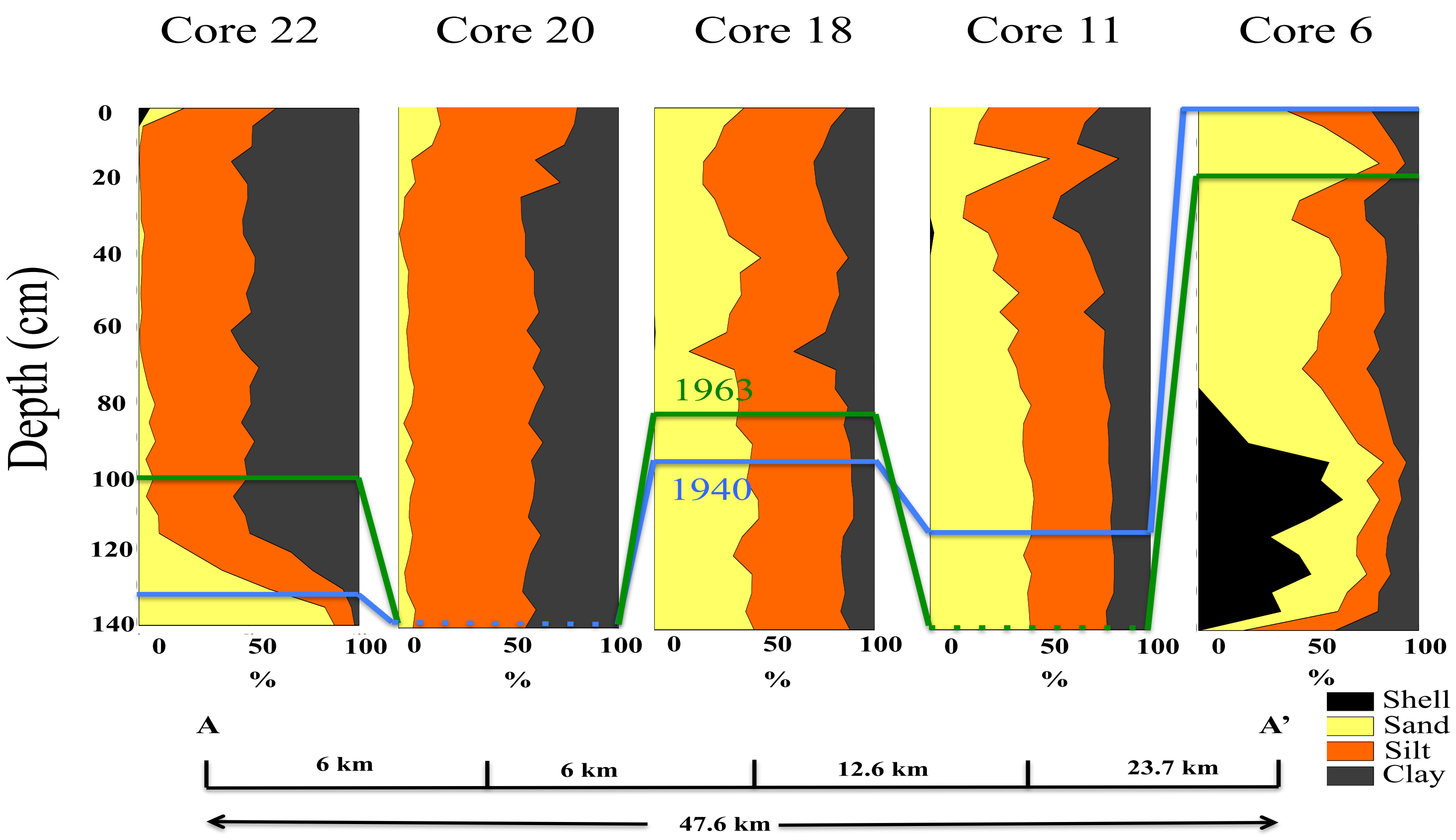

Figure 24. Cross-section through core 22 to core 6 in Galveston Bay. The correlation based on radionuclide dating and the depth of background level of Hg. Transect location is shown in figure 1 (cross section A-A’). The dashed line indicates that the correlation is missing. blue line indicates 1940s, and green line indicate the maximum depth of ^{137}Cs. The grain size composition is represented as relative percentage. Distance between cores is indicated in km.

4.5 Recent Hg fluxes and Hg inventory

The present-day Hg fluxes to the surface sediment and the total and anthropogenic inventories for the upper 140 cm were calculated for all locations (Table 2). Hg flux (ng m^{-2} yr^{-1}) was calculated using the following equation [*Covelli et al*, 2012]:

$$\text{Hg flux} = (1 - \phi) * S * \rho * \text{T-Hg} \quad (3)$$

Where S is the sediment accumulation rate (cm yr^{-1}), T-Hg is the total Hg concentration (ng g^{-1}) and ρ is the sediment density (g cm^{-3}). The calculated results (figure 25) show low fluxes of Hg in the southern and eastern side of the bay (core 3, 6 and 9). On the other hand, in upper part of the bay, especially within the SJR/HSC and the Core 11 location, there is a high Hg flux. In general, there is a gradient of Hg flux in Galveston Bay, being high in SJR/HSC and decrease toward GOM. The surface flux results reflect the influence of the anthropogenic activities along SJR/HSC. In 2001, Santschi et al, estimated the present-day flux of Hg to the surface sediment to be 13.6 ng cm^{-2} yr^{-1} in Trinity Bay. However in this study, the present-day flux of Hg in Trinity Bay is 6.1 ng cm^{-2} yr^{-1}. The decrease in Hg fluxes reflects the amount of Hg being released and the regulations requiring the decreased the input of Hg to the system.

The anthropogenic concentration of Hg to the system was calculated by the difference between the total concentration of Hg and the background concentration:

$$\text{AR Hg} = (\text{T-Hg}) - (\text{Background Hg}) \quad (4)$$

Within most cores, there is evidence of the anthropogenic input of Hg, with a clear increase around 1940.

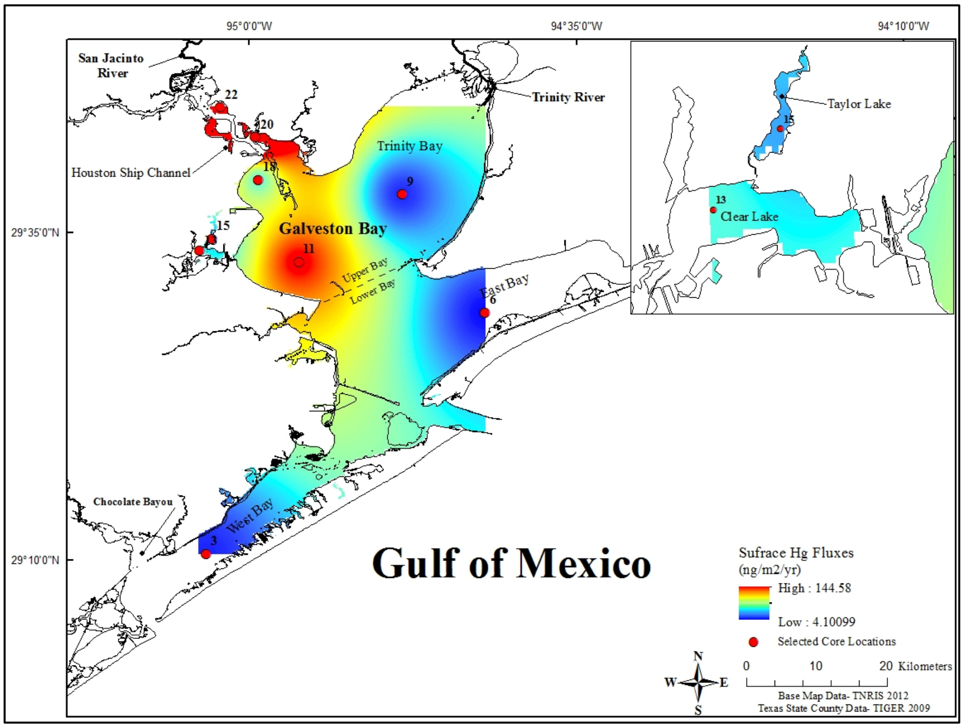

Figure 25. Areal distribution of present-day Hg fluxes to the surface sediment for all locations in Galveston Bay.

Hg inventory (ng m^{-2}) represents the total amount of Hg being loaded to the sediment over a period of time and deposited over a surface area (*Kolak et al*, 1998). The following equation was used to calculate the amount of Hg buried in the sediment:

$$\text{Hg Inv} = \Sigma\, [\text{T-Hg} * (1-\phi) * \rho * d] \qquad (5)$$

Where d is the thickness of the sediment between consecutive depth levels (cm). Figure 18, and 19 represent the total and anthropogenic inventories of Hg for the upper 140 cm.

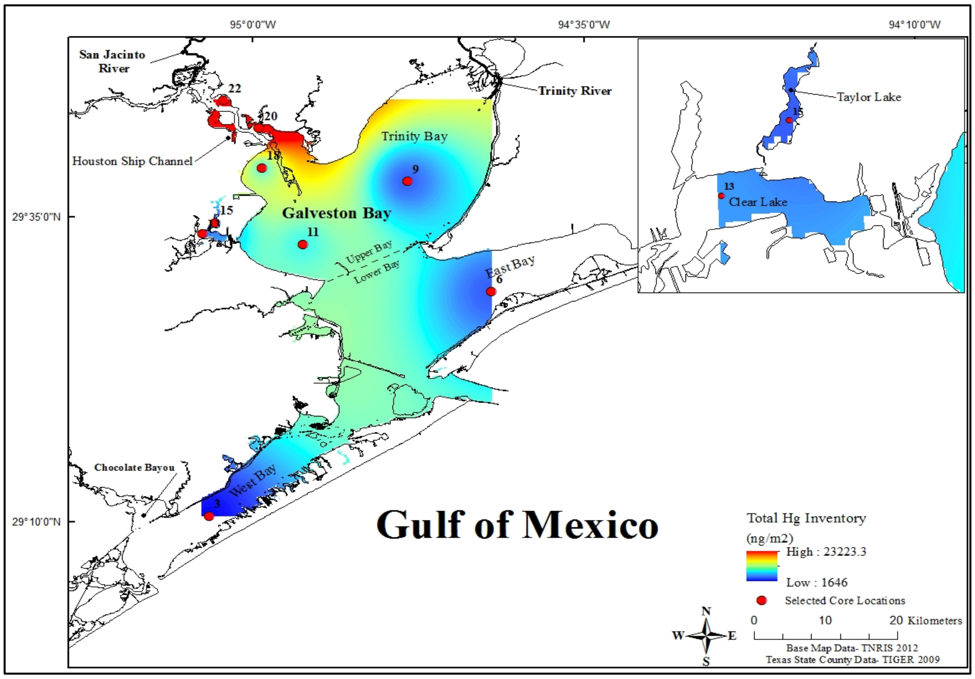

Figure 26. Areal distribution of total Hg inventory (upper 140 cm)

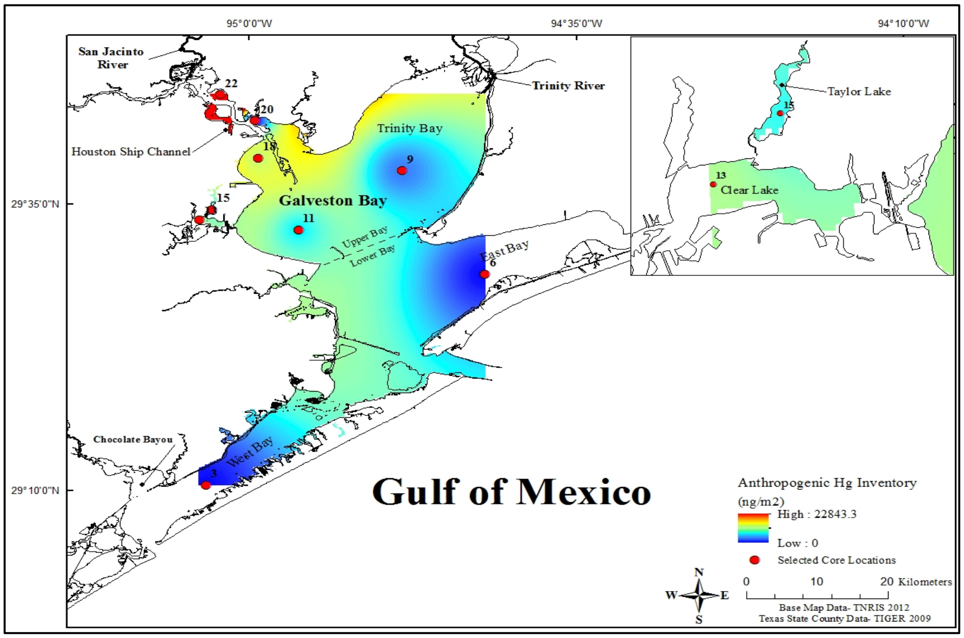

Figure 27. Areal distribution of anthropogenic Hg inventory (upper 140 cm)

Results from the total inventory (figure 26) show a significant difference between areas around SJR/HSC and the southern side of the bay (table 1). The accumulation of total Hg is higher in SJR/HSC (23228 ng m^{-2}) and decreases towards GOM (2169 ng m^{-2}). In contrast, although the distribution of anthropogenic inventories (figure 27) of Hg follows the same trend as the total inventories being high in the upper section of the bay and decreasing seaward, the anthropogenic inventory for Cores 3 and 6 were zero and very low for core 9, indicating that most Hg is being trapped in the upper part of the bay and the western side and less Hg has been trapped in East and West Bay. The results confirm that areas with highest rates of fluxes and inventories are a preferential accumulation sites for anthropogenic Hg.

Additionally, the results show that areas with higher land subsidence rate such as Core 22 (2.4 cm yr^{-1}), also have higher sedimentation rate on average (1.86 cm yr^{-1}), and have higher inventories and fluxes of Hg (Table 2) compare to locations where the land subsidence rate and sediment accumulation rate are low (Core 3) and where there is higher wave energy and coarser grain size fraction is dominant.

5. CONCLUSIONS

Galveston Bay is an ideal site to investigate the ability for an estuary to keep pace with rapid sea level rise and land subsidence as well as the implications this has in terms of contaminant fate and transport of particle bound contaminants such as Hg. The areas around the bay, especially SJR/HSC, are intensely industrialized and contain one of the largest petroleum and chemical industrial complexes in the world. As a results groundwater withdraw to support these industries as well as the growing population, the bay experienced a gradient of elevated land subsidence, with higher land subsidence rate in SJR/HSC (3 cm yr^{-1}) and decreasing seaward towards Galveston Island (0.6 cm yr^{-1}).

Sedimentation rate in the bay was obtained using short-lived isotopes (^{210}Pb and ^{137}Cs), and the results indicate a higher sedimentation rates in SJR/HSC area and decreasing rates toward the GOM. Sedimentation rates are high in areas with higher land subsidence rates, although the sedimentation rates are lower than subsidence rates. However, when relative sea level rise is factored in, overall, sedimentation generally did not kept pace with RSLR, although they have the same relative order.

The sedimentation rates, when correlated with Hg core profiles show significant input of Hg beginning around 1940, indicating that Hg can be a valuable geochronological tool. In general, the sedimentation rate obtained using Hg is in a good agreement with the other dating methods, demonstrating that Hg concentration profiles have utility as a geochronology tool when used in conjunction with excess ^{210}Pb, and ^{137}CS geochronologies, in areas with a historically high input of Hg. The concentration, inventory, and fluxes of Hg profiles show higher values in areas proximal to the SJR/HSC and progressively decreasing seaward and to distal parts of the bay, which reflects the anthropogenic emission from SJR/HSC. Furthermore, areas with higher land subsidence rates and sedimentation rate have a higher inventory of contaminants such as Hg.

Overall, the results of this study demonstrate that sedimentation rates within Galveston Bay are the same ratio as LSR and RSLR rates, ranging from 14% and 121% higher than sedimentation rates. Although the reasons for these differences vary between sites and the error associated with estimations of land subsidence rates vary depending on the distance from monitoring stations, it appears that in general, sedimentation is lagging behind RSLR. Additionally, areas with higher sedimentation/RSL rates are also areas with dramatically higher inventories of Hg, suggesting that these areas also contain dramatically higher inventories of other particle bound contaminants.

REFRERENCES

Acquavita, A., S. Covelli., A. Emili., D. Berto., J. Faganeli., M. Giani., M. Horvat., N. Koron., and F. Rampazzo (2012), Mercury in the sediment of the Marano and Grado Lagoon (Northern Adriatic Sea): Sources, distribution and speciation, Estuarine, Coastal and Shelf Science, **113**, 20-31.

Bank, M (2012), Mercury in the Environment: Pattern and Processes, 1st edn, University of California Press, Berkeley.

Barbeau, C., R. Bougie., and J-E. Cote (1981), Temporal and spatial variations of mercury, lead, zinc, and cooper in sediment of the Saguenay Fjord, Canadian Journal of Earth Sciences, **18**, 1065-1074

Baskaran M., and S. Naidu (1995), ^{210}Pb-derived chronology, and the fluxes of ^{210}Pb and ^{137}Cs isotopes into continental shelf sediments, East Chukchi Sea, Alaskan Arctic, Geochimica et Cosmochimica Acta **59**, 4435-4448.

Bianchi, T. S (2007), Biogeochemistry of Estuaries, Oxford University Press, New York, New York.

Burdige, D. J (2006), Geochemistry of Marine Sediments, Princeton University Press, Princeton, New Jersey.

ChemPlants, (2013), Houston Ship Channel Map, Available from ChemPlants (http://fatsnake.com/homesite/Active.asp?Reg=HSC&sFolder=/Maps).

Clampet. A. P (2012), Methylmercury: Formation, Sources and Health Effects, 1st ed, Nova Science Publishers, New York, New York.

Coplin, L.S., and D. Galloway (1999), Houston-Galveston, Texas—Managing coastal subsidence, Land subsidence in the United States: U.S. Geological Survey Circular **1182**, 35–48.

Covelli, S., L. Langone., A. Acquavite., R. Piani., and A. Emili (2012), Historical flux of mercury associated with mining and industrial sources in the Marano and Grado Lagoon (Northern Adriatic Sea), Estuarine, Coastal and Shelf Science, **113**, 1-13. Doi:10.1016/j.ecss.2011.12.038.

Dalrymple, R.W., B. A. Zaitlin., and R. Boyd (1992), Estuarine facies models: conceptual basis and stratigraphic implications, Journal of Sedimentary Petrology, **62**, 1130–1146.

Di Leonardo, R., G. Tranchida., A. Bellanca., R. Neri., M. Angelone., and S. Mazzola (2006), Mercury level in sediments of central Mediterranean Sea: A 150+ year record from box-cores recovered in the Strait of Sicily, Chemosphere. **65**, 2366-2376.

Ding, Z. H., J. L. Liu., L. Q. Li., H. N. Lin., H. Wu., and Z. Z. Hu (2009), Distribution and speciation of mercury in surficial sediments from main mangrove wetlands in China, Marine Pollution Bulletin **58**, 1319-1325.

EPA (Environmental Protection Agency) (1998), Method 7473: Mercury in Solids and Solutions by Thermal Decomposition, Amalgamation, and Atomic Absorption Spectrophotometry, EPA SW-846 Cincinnati, USEPA Office of Research and Development Environmental Monitoring Systems Laboratory.

EPA (Environmental Protection Agency) (2007), National Estuary Program Coastal Condition Report, Chapter: Gulf of Mexico National Estuary Program Coastal Condition, Galveston Bay Estuary Program.

EPA (Environmental Protection Agency) (2010), Sea Level: Climate Change: US EPA, Available at (http://www.epa.gov/climatechange/science/indicators/oceans/sea-level.html).

Faure, G. and T. M. Mensing (2005), Isotopes Principles and Applications, edn. 3, John Wiley & Sons, Inc., Hoboken, New Jersey.

Figueres, G., J. M. Martin, M. Meybeck, and P. Seyler (1985), A comparative study of mercury contamination in the Tagus estuary (Portugal) and major French estuaries (Gironde, Loire, Rhône), Estuarine, Coastal and Shelf Science, **20**, 183-203.

Gardinali, P.R (1996), Assessment of halogenated aromatic compounds contamination in the Galveston Bay ecosystem, Ph.D. Dissertation, Texas A&M University, College Station, TX.

GBNEP (Galveston Bay National Estuary Program) (1992), Ambient water and sediment quality of Galveston Bay: present status and historical trends, Galveston Bay National Estuary Program Publication (GBNEP), 22.

GBNEP (Galveston Bay National Estuary Program) (1994), The State of the Bay: a characterization of the Galveston Bay Ecosystem. Galveston Bay National Estuary Program Publication (GBNEP), 44.

Google Earth (2013) Map of Galveston Bay-Scott Bay. Available at (http://www.google.com/earth/index.html)

Han, S., G. A. Gill., R. D. Lehman., and K. Choe (2006), Complexation of mercury by dissolved organic matter in surface water of Galveston Bay, Texas, Marine Chemistry, **98**, 156-166.

Han, S., R. D. Lehman., K. Choe., and G. A. Gill (2007), Chemical and physical speciation of mercury in Offatts Bayou: A seasonally anoxic bayou in Galveston Bay, Limnology and Oceanography, **52(4)**, 1380–1392.

Harmon, M., A. S. Pait, and M. J. Hameedi (2003), Sediment Contamination, Toxicity, and Macroinvertebrate Infaunal Community in Galveston Bay. NOAA Tech. Memo. NOS NCCOS CCMA 122. Silver Spring, MD: NOAA, NOS, Center for Coastal Monitoring and Assessment.

HGSD (Houston Galveston Subsidence District) (2008), Subsidence: 1906–2000. available at (http://www.subsidence.org/Assets/PDFDocuments/)

HGSD (Houston Galveston Subsidence District) (2013) Introduction to subsidence and groundwater regulation, available at (http://www.hgsubsidence.org/assets/pdfdocuments/QApamphletIntro.pdf).

Hu, R. L., Z. Q. Yue., L. C. Wang., and S. J. Wang (2004), Review on current status and challenging issues of land subsidence in China, Engineering Geology, **76**, 65-77.

Jason, J. and M. Baskaran (2011), Interconnected riverine–lacustrine systems as sedimentary repositories: Case study in southeast Michigan using ^{210}Pb and ^{137}Cs-based sediment accumulation and mixing models, Journal of Great Lakes Research, **37**, 432-446.

Kading, t. J., R. P. Mason., and J. J. Leaner (2009), Mercury contamination history of an estuarine flooding reconstructed from a ^{210}Pb sediment core (Berg River, South Africa), Marine Pollution Bulletin, **59**, 116-122.

Kasmarek, M.C., M. R. Johnson., and J. K. Ramage (2010), Water-level altitudes 2010 and water-level changes in the Chicot, Evangeline, and Jasper aquifers and compaction 1973–2009 in the Chicot and Evangeline aquifers, Houston- Galveston region, Texas:U.S. Geological Survey Scientific Investigations Map 3138, 16 p, 17 sheets.

Kolak, J. J., D. T. Long., and T. M. Beals (1998), Anthropogenic inventories and historical and present accumulation rates of copper in Great Lakes sediment. Applied Geochemistry, **13**, 59-75.

Lasorsa, B. K., G. A. Gill., and M. Horvat (2012), Analytical methods for measuring mercury in water, sediment, and biota, Chapter 3 from: Mercury in the Environment: Pattern and Processes, 1st edn, edited by Bank, M (2012), University of California Press, Berkeley.

Lee, A., S. Han., and G. Gill (2011), Estuarine mixing behavior of colloidal organic carbon and colloidal mercury in Galveston Bay, Texas, Journal of Environmental Monitoring, DOI: 10.1039/c0em00666a.

Lester, L. J. and L. A. Gonzalez (2011), The State of the Bay: A Characterization of the Galveston Bay Ecosystem, Third Edition, Texas Commission on Environmental Quality, Galveston Bay Estuary Program, Houston, Texas.

Liu, G., Y. Cai., and N. O'Driscoll (2012) Environmental Chemistry and Toxicology of Mercury, John Wiley and Sons, New Jersey

Lockwood, R.A., and K.Y. Chen (1973), Adsorption of Hg (II) by hydrous manganese oxides, Environmental Science and Technology, **7**, 1028-1034

Louchouarn, P., and M. Lucotte (1998) A historical reconstruction of organic and inorganiccontamination events in the Saguenay FjordrSt. Lawrence system from preindustrial times to the present, The Science of the Total Environment, **213**, 139-150.

MacKenzie, A. B., S. M. L. Hardie, J. G. Farmer, L. J. Eades, and I. D. Pulford (2011), Analytical and sampling constraints in ^{210}Pb dating, Science of the Total Environment, **409**, 1298-1304.

Menounou, N. and B. J. Presley (2003), Mercury and Other Trace Elements in Sediment Cores from Central Texas Lakes, Environmental Contamination Toxicology, **45**, 11-29, DOI: 10.1007/s00244-002-2120-4

Morse, J. W., B. J. Presley., and R. J. Taylor (1993), Trace Metal Chemistry of Galveston Bay: Water, Sediment and Biota. Marine environmental Research, **36**, 1-37.

Neff, J. M (2002), Bioaccumulation in marine organisms, effect of contaminants from oil well produced water, 1st ed, Elsevir science Ltd, San Deigo, USA

Nichols, G (2009), Sedimentology and Stratigraphy, 2 edn, Wiley Blackwell, Uk.

Nittrouer, C.A., J. A. Austin, M. E. Field, J. H. Kravitz, J. P. Syvitski, and P. L. Wiberg. (2007), Writing a Rosetta stone: insights into continental-margin sedimentary processes and strata in continental Margin Sedimentation: from Sediment Transport to Sequence Stratigraphy, Special publication number 37 of the International Association of Sedimentologist, edited by Nittrouer et al., 1-48, Blackwell Publishing, Malden, MA, USA.

Nittrouer, C.A., Sternberg, R.W., Carpenter, R., Bennett, J.T (1979), The use of Pb-210 geochronology as a sedimentological tool: Application to the Washington continental shelf, Marine Geology, **31**, 297-316.

Ravens, T. M., R. C. Thomas., K. A. Roberts., and P. H. Santschi (2009), Causes of Salt Marsh Erosion in Galveston Bay, Texas, Journal of Coastal Research, **25**, 265-272.

Rodriguez, A. B., Anderson, J. B., and Simms, A. R (2005), Terrace inundation as an autocyclic mechanism for parasequence formation: Galveston estuary, Texas, U.S.A., Journal of Sedimentary Research*,* **75**, 608-620.

Sanders, R. D., K. H. Coale., G. A. Gill., A. H. Andrews., and M. Stephenson (2008), Recent increase in atmospheric deposition of mercury to California aquatic systems inferred from a 300-year geochronological assessment of lake sediments, Applied Geochemistry, **23**, 399-407.

Santschi, P. H., B. J. Presley, T. L. Wade, B. Garcia-Romero, and M. Baskaran (2001), Historical contamination of PAHs, PCBs, DDTs, and heavy metals in Mississippi River Delta, Galveston Bay and Tampa Bay sediment cores, Marina Environmental Research, **52**, 51-79.

Santschi, P.H, M. A. Allison, S. Asbill, A. B. Perlet, S. Cappellino, C. Dobbs, and L. MCshea, (1999), Sediment Transport and Hg Recovery in Lavaca Bay, as Evaluated from Radionuclide and Hg Distributions, Environmental Science and Technology, **33**, 378-391.

Sharma, P., L.R. Gardner, W.S. Moore, and M.S. Bollinger (1987), Sedimentation and Bioturbation in a salt marsh as revealed by ^{210}Pb, ^{137}Cs, And ^{7}Be studies, Limnology and Oceanography, **32**, 313-326.

Shi, J., C. C. M. Ip., G. Zhang., G.Jiang., and X. Li (2010), Mercury profile in sediments of the Pearl River Estuary and the surrounding coastal area of South China, Environmental Pollution, **158**,1974-1979.

Sibley, T. H., and J. J. Morgan (1977), Equilibrium speciation of trace metals in fish water: seawater mixtures/ Proc. International Conference on Heavy Metals in the Environment. Toronto, Canada, **1**, 319-338

USGS (United State Geological Survey) (2002), Houston-Galveston Bay Area, Texas, From Space - A New Tool for Mapping Land Sub, USGS Fact Sheet 110-02, Available at (http://pubs.usgs.gov/fs/fs-110-02/pdf/FS_110-02.pdf).

Van Metre, P., J. T. Wilson., C. C. Fuller., E. Callender., and B. J. Mahler (2004), Collection, Analysis, and Age-Dating of Sediment Cores From 56 U.S. Lakes and Reservoirs Sampled by the U.S. Geological Survey, 1992–2001, National Water-Quality Assessment Program. Scientific Investigations Report 2004–5184. U.S. Department of the Interior and U.S. Geological Survey

Warner, J. C., B. Butman, and P. S. Dalyander (2008), Storm-driven sediment transport in Massachusetts bay, Continental shelf Research, **28**, 257–282

Wen, L., P. Santschi., G. Gill., and C. Paternostro (1999), Estuarine trace metal distributions in Galveston Bay: importance of colloidal forms in the speciation of the dissolved phase, Marine Chemistry, **63**, 185-212.

Windom, H. L., S.J. Schropp., F. D. Calder,., J. D. Ryan., R. G. Smith Jr., L. C. Burney., F. G. Lewis., and C. H. Rawlinson (1989), Natural trace metal concentration in estuarine and coastal marine sediments of the southeastern United States, Environmental Science and Technology, **23**, 341-320.

Yeager, K. M., P. H. Santschi., H. S. Rifai.,M. P. Suarez., R. Brinkmeyer., C. Hung., K. J. Schindler., M. J. Andres., and E. A. Weaver. (2007), Dioxin Chronology and Fluxes in Sediments of the Houston Ship Channel, Texas: Influence of Non-steady-State Sediment Transport and Total Organic Carbon, Environmental Science and Technology, **41**, 5291-5398.

Yeager, K. M., P. H. Santschi, and G. T. Rowe. (2004), Sediment accumulation and radionuclide inventories (^{239,240}Pu,^{210}Pb and ^{234}Th) in the northern Gulf of Mexico, as influenced by organic matter and macrofaunal density, Marine Chemistry, **91**, 1-14.

Yeager, K. M., R. Brinkmeyer., C. F. Rakocinski., K. J. Schindler., and P. H. Santschi. (2010), Impacts of Dredging Activities on the Accumulation of Dioxins in Surface Sediments of the Houston Ship Channel, Texas, Journal of Coastal Research, **62**, 743-752.

Yuill, R. M (1991), A paleoecological Study of a one-hundred year sedimentary record of Galveston Bay, Texas, Ph. D. Dissertation, Texas A and M University, College Station, TX.

Zilkowski, D.B., Hall, L.W., Mitchell, G.J., Kammula, V., Singh, A., Chrismer, W.M., and Neighbors, R.J (2003), The Harris-Galveston Subsidence District/National Geodetic Survey Automated Global Positioning System Subsidence Monitoring Project: Harris-Galveston Subsidence District, Friendswood, Tex, available at (http://www.hgsubsidence.org/assets/pdfdocuments/GPSProject.pdf)

APPENDIX A

POROSITY AND CORE PHOTOGRAPHS

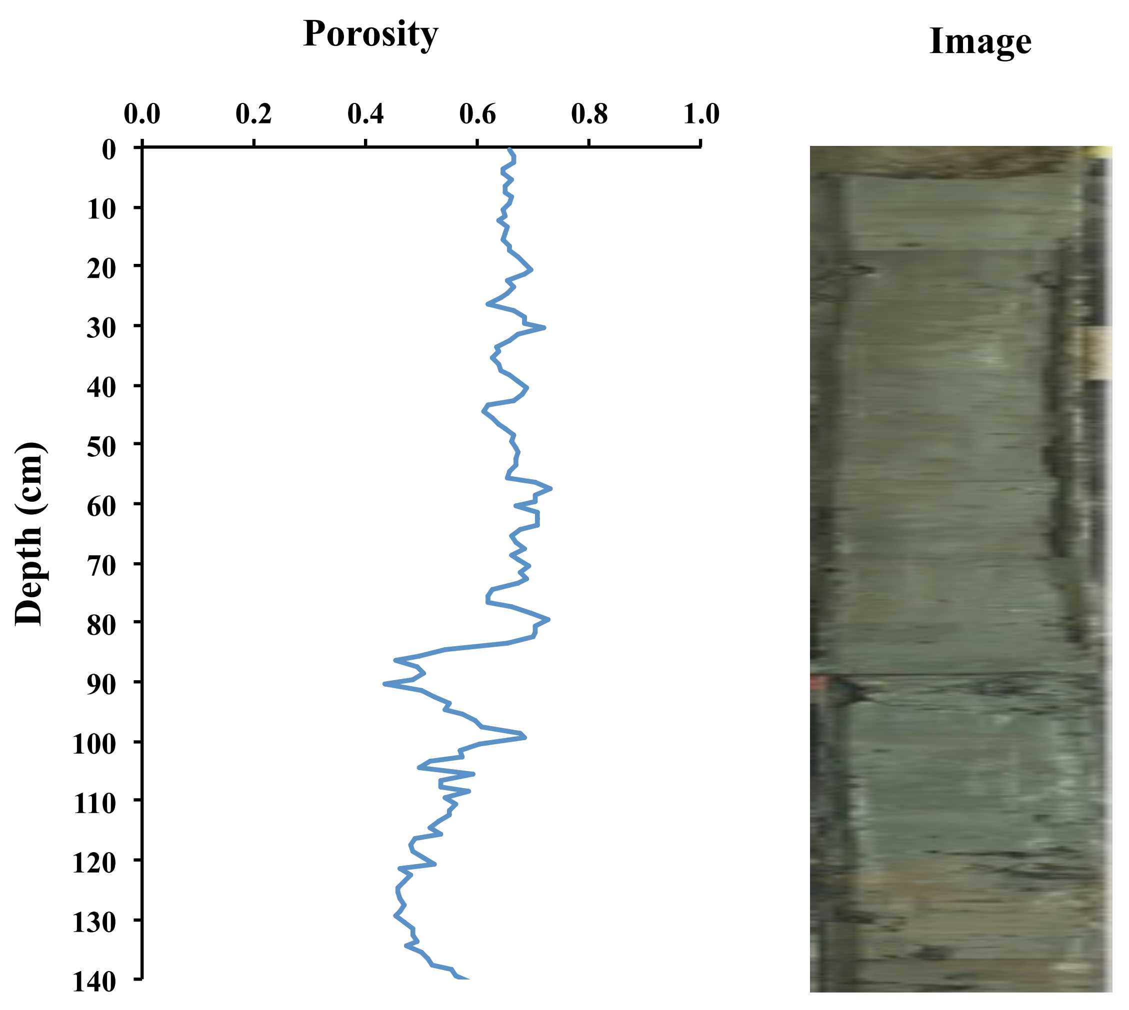

Figure A1. Porosity profile and core photograph for site 3 – West Galveston Bay

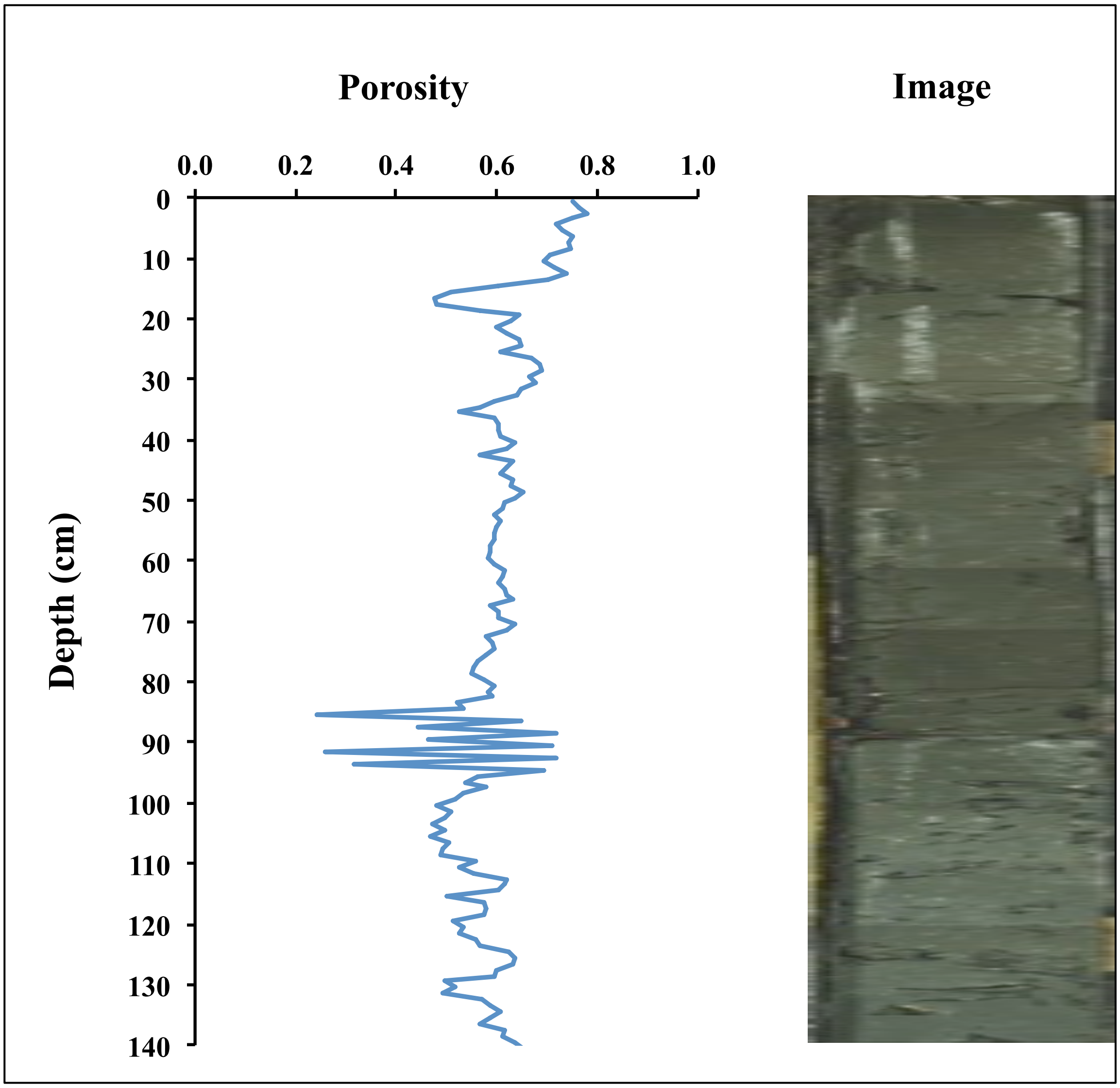

Figure A2. Porosity profile and core photograph for site 6 – East Galveston Bay

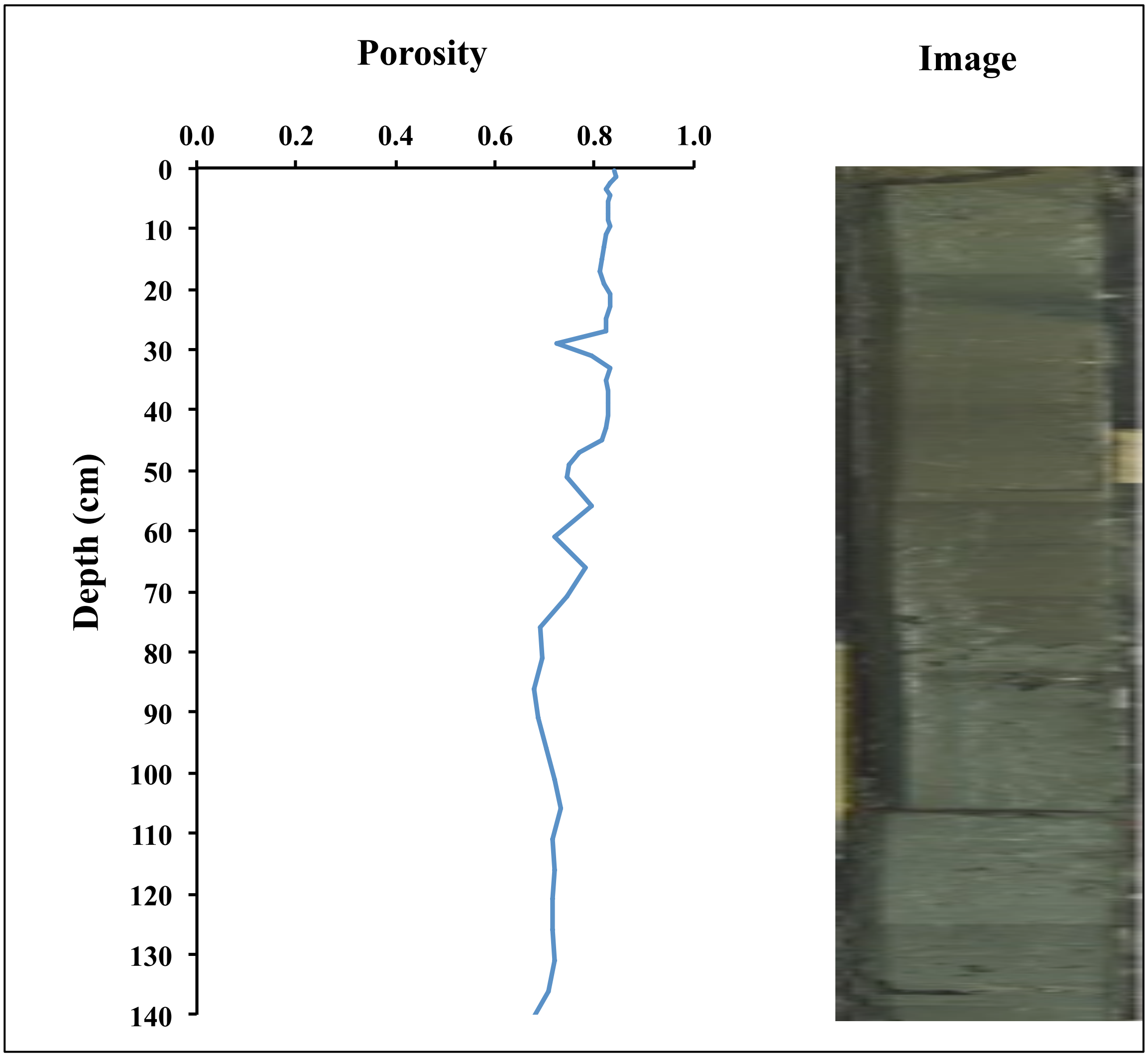

Figure A3. Porosity profile and core photograph for site 9 – Trinity Bay

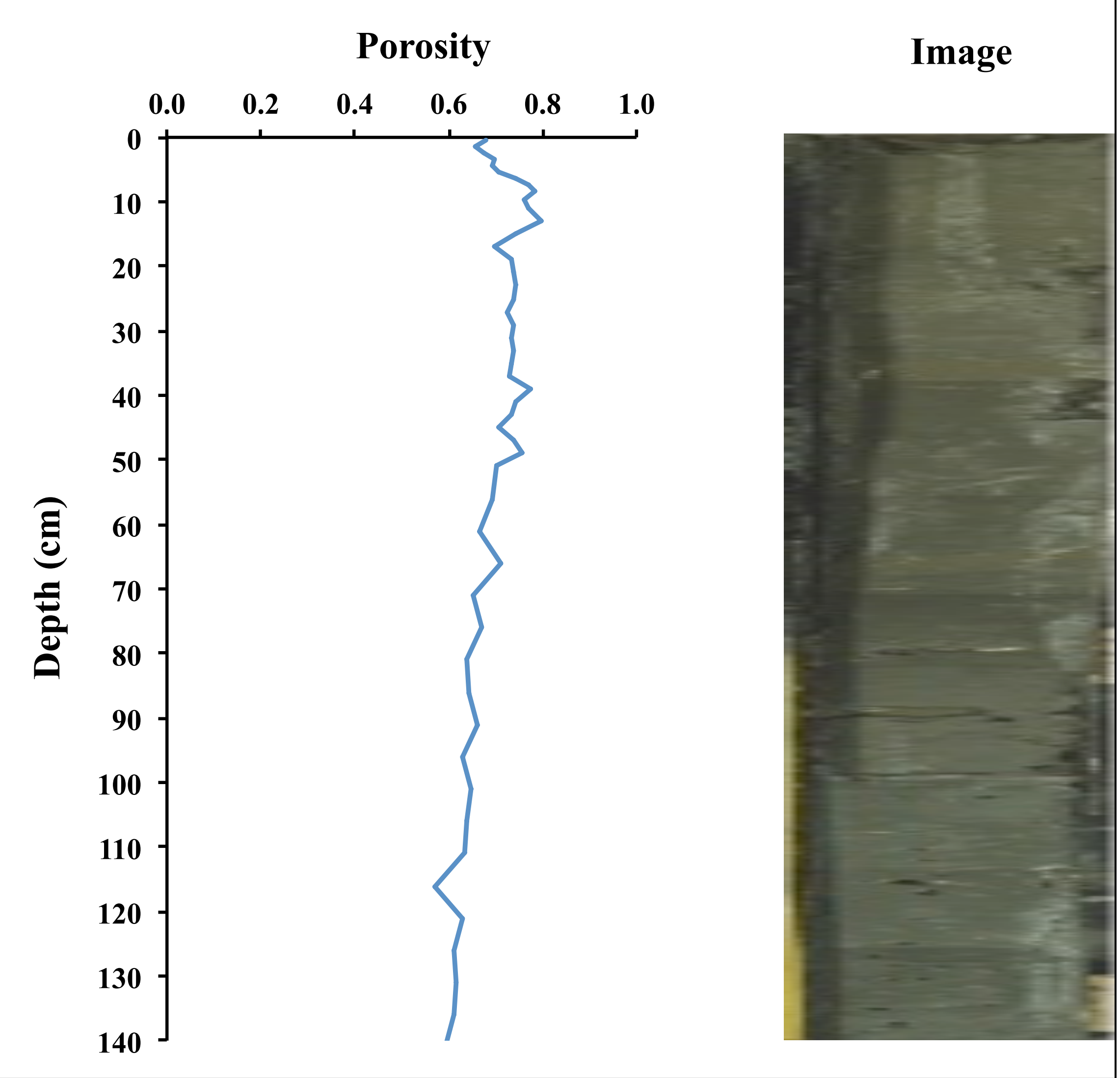

Figure A4. Porosity profile and core photograph for site 11 – Upper Galveston Bay

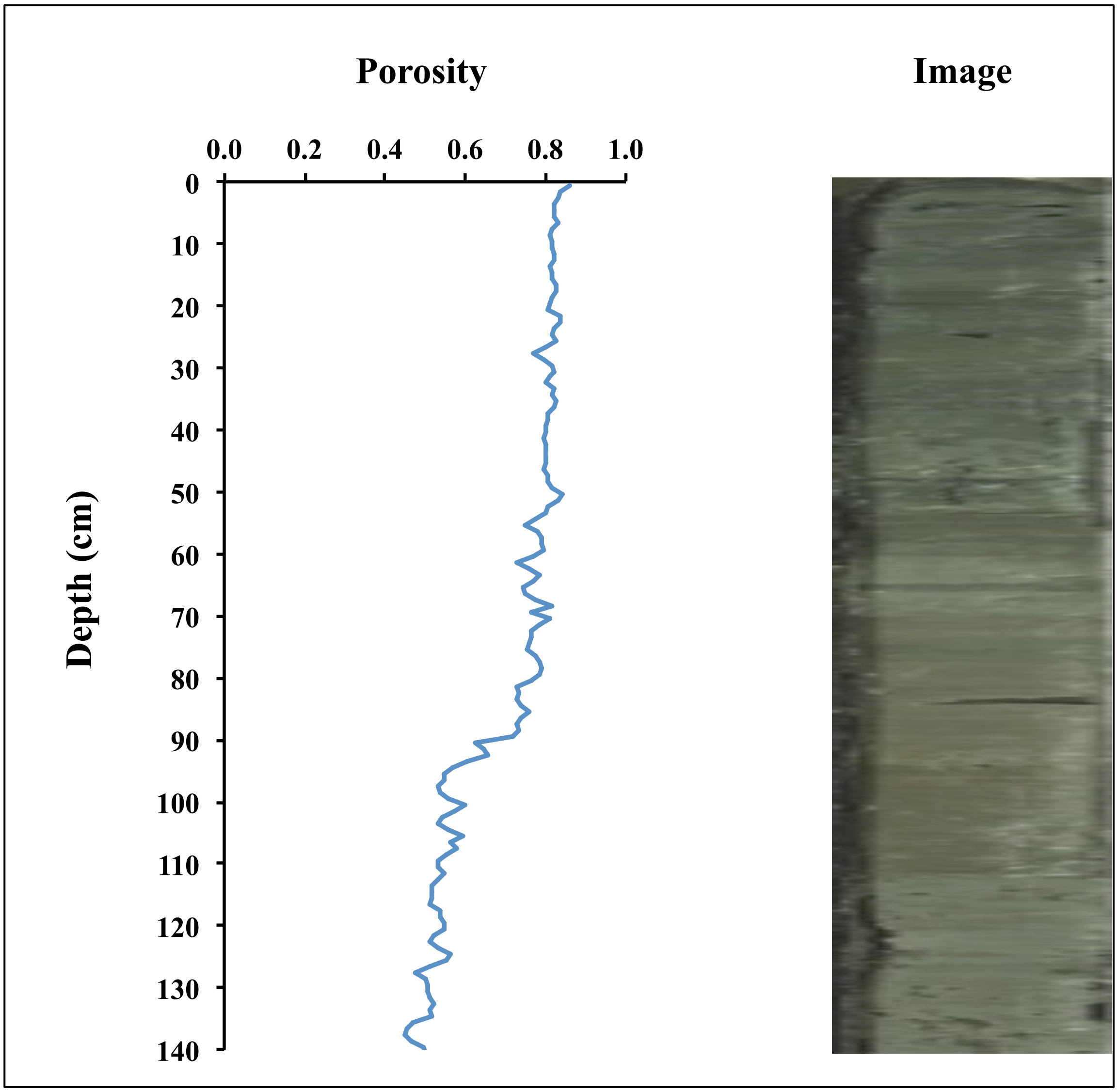

Figure A5. Porosity profile and core photograph for site 13 – Clear Lake

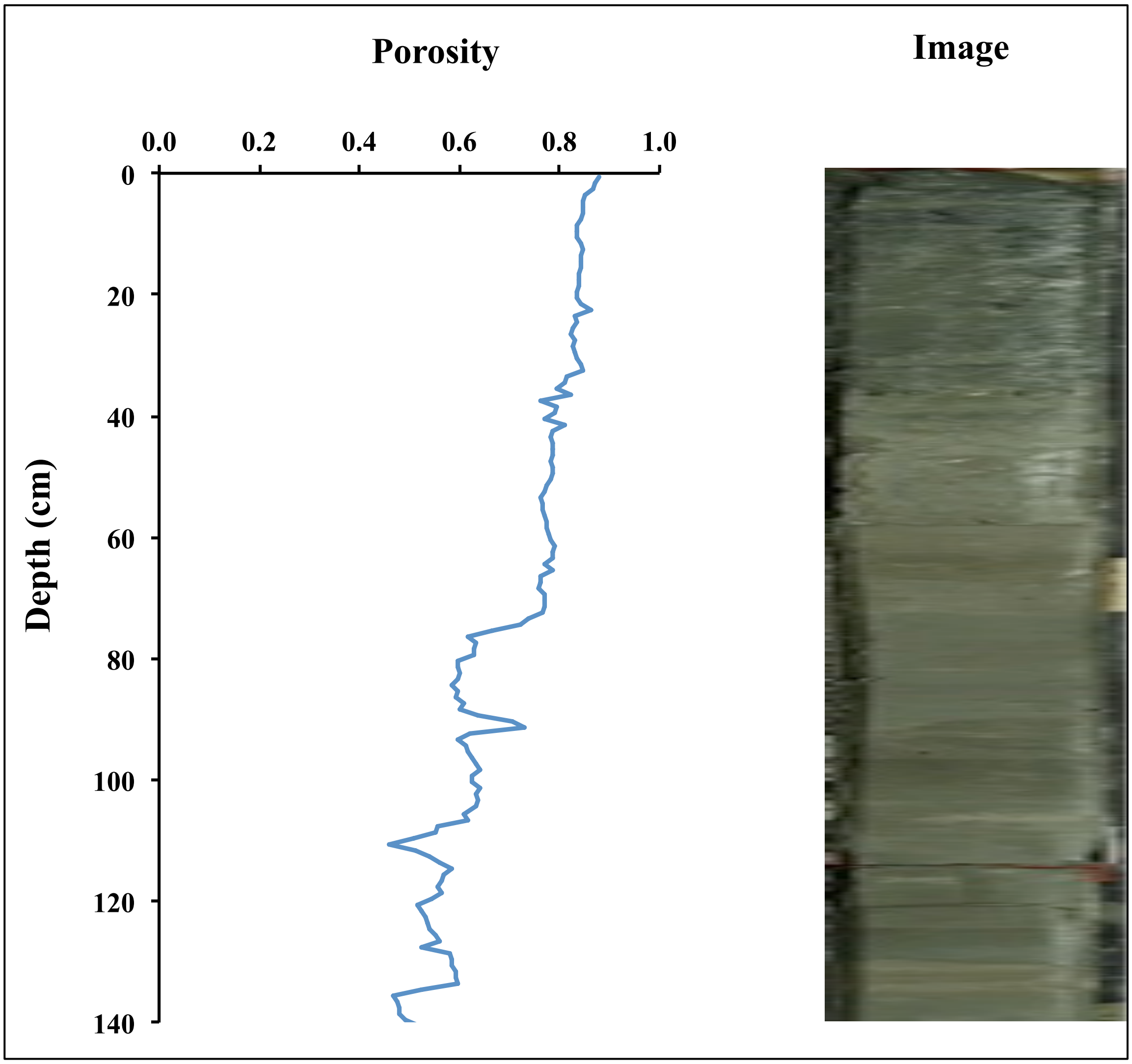

Figure A6. Porosity profile and core photograph for site 15 – Taylor lake

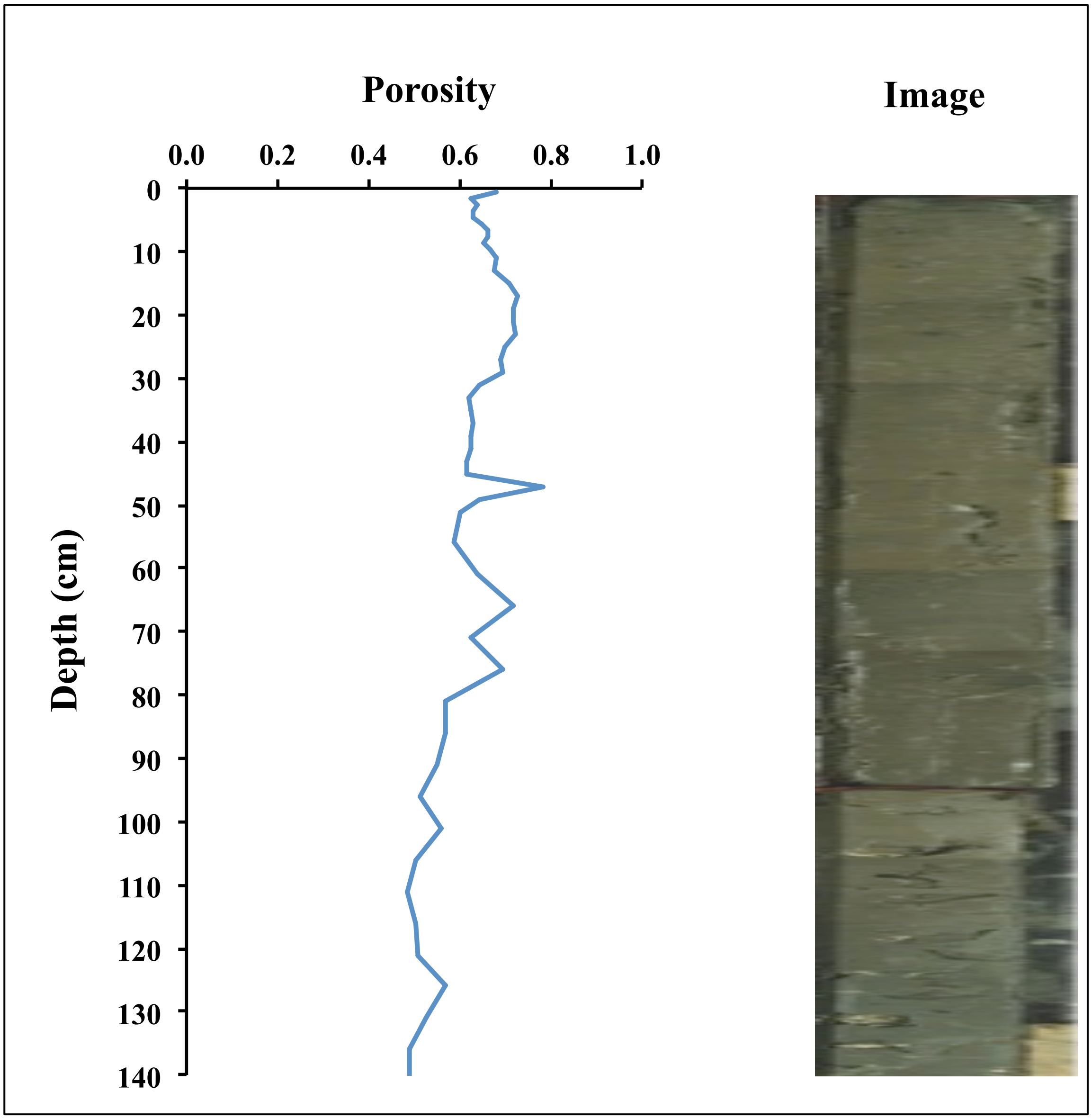

Figure A7. Porosity profile and core photograph for site 18 – Upper Galveston Bay

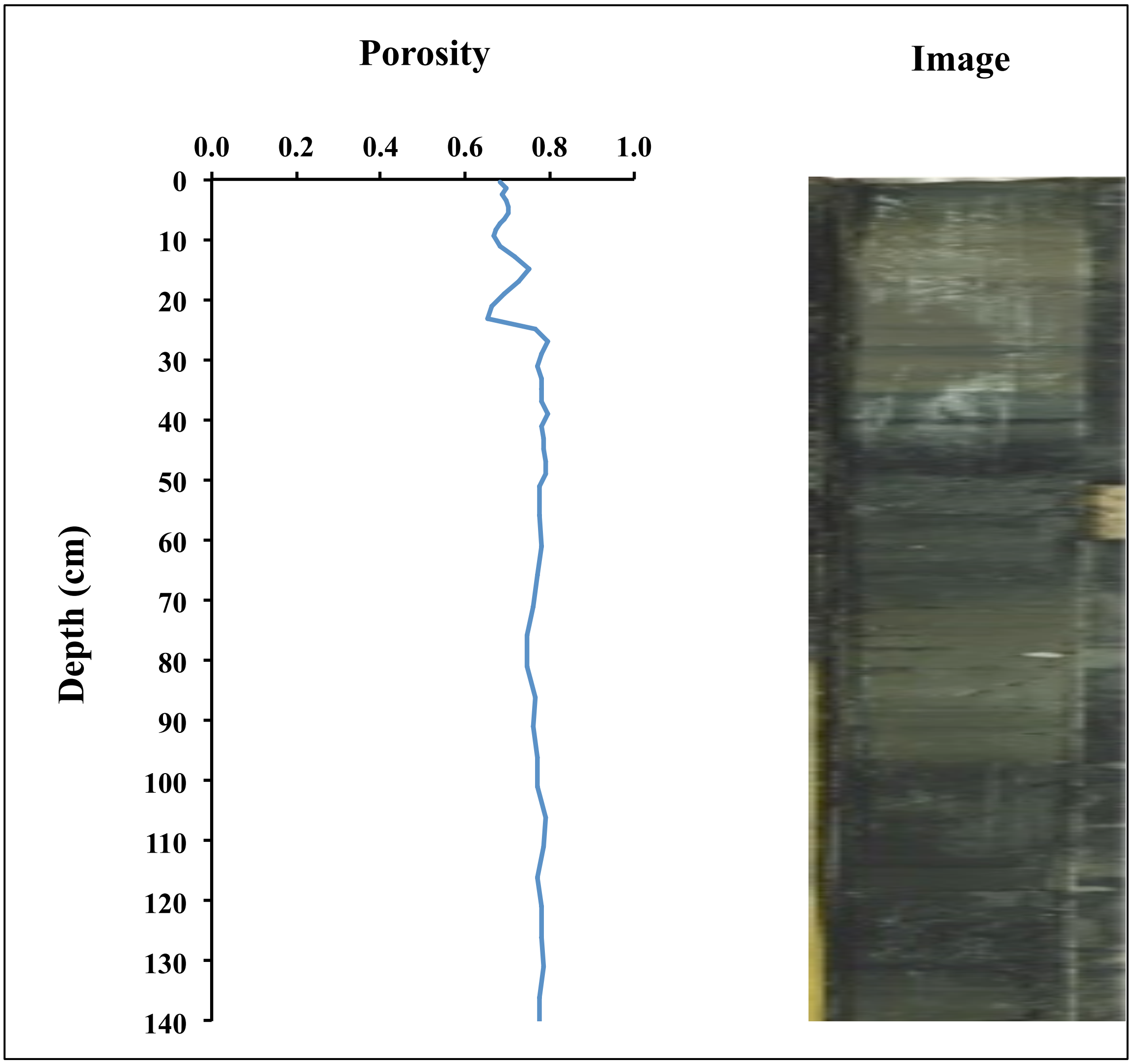

Figure A8. Porosity profile and core photograph for site 20 – Tabbs Bay

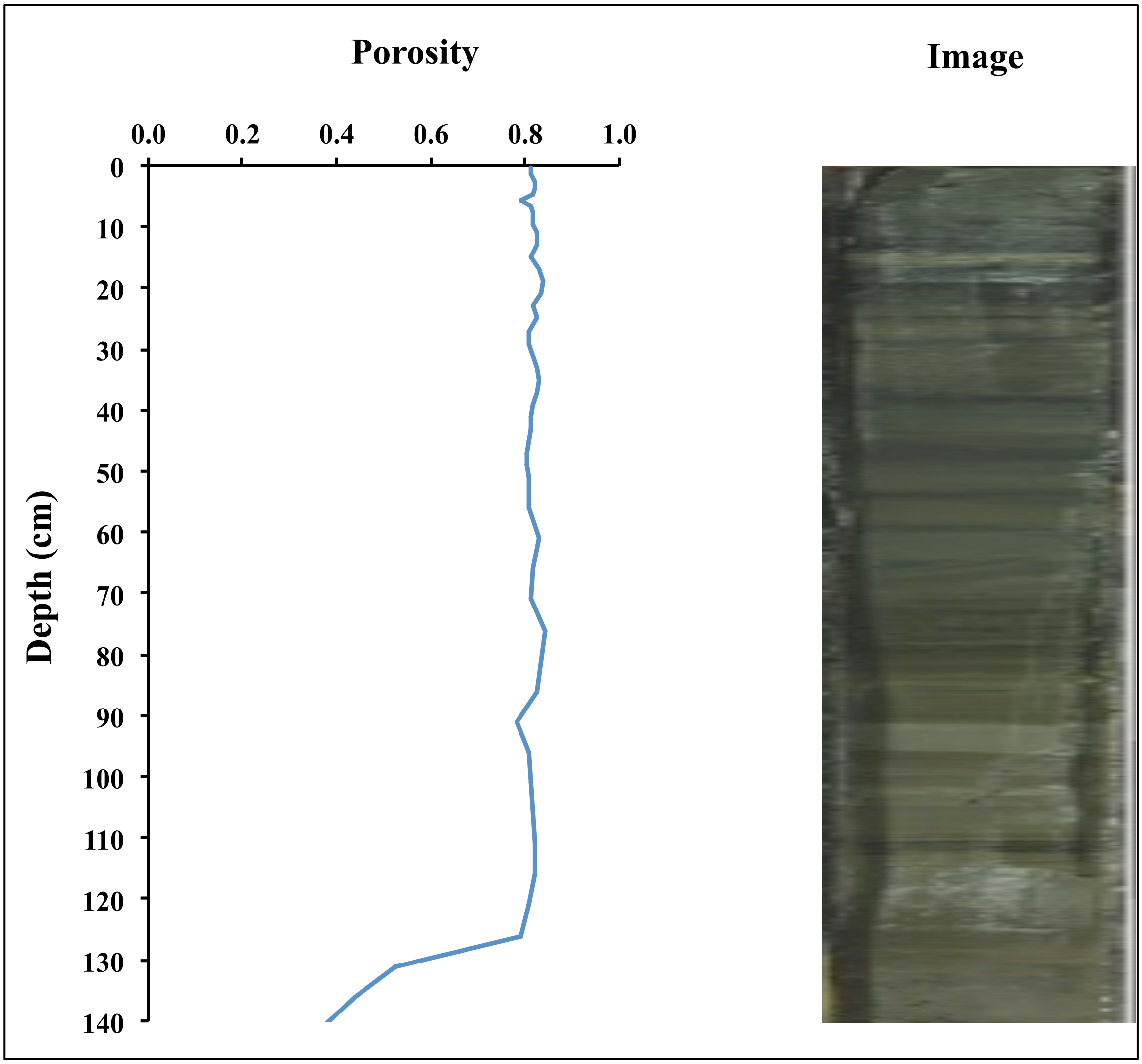

Figure A9. Porosity profile and core photograph for site 22 – Scott Bay

APPENDIX B
MERCURY AND GRAIN SIZE CORRELATION

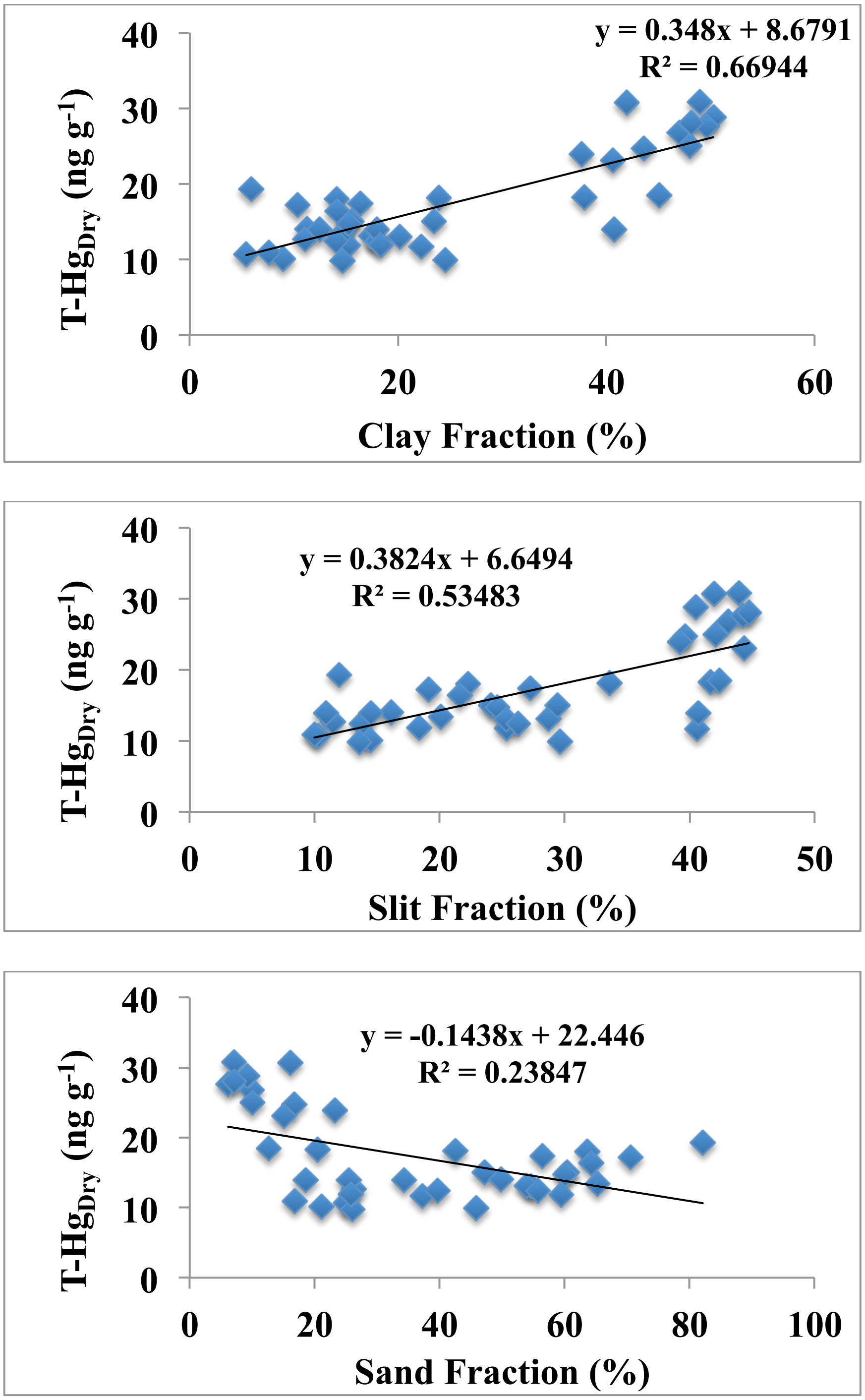

Figure B1. Correlation between Hg concentration and the percentage of grain size fraction in coring site 6 – East Galveston Bay.

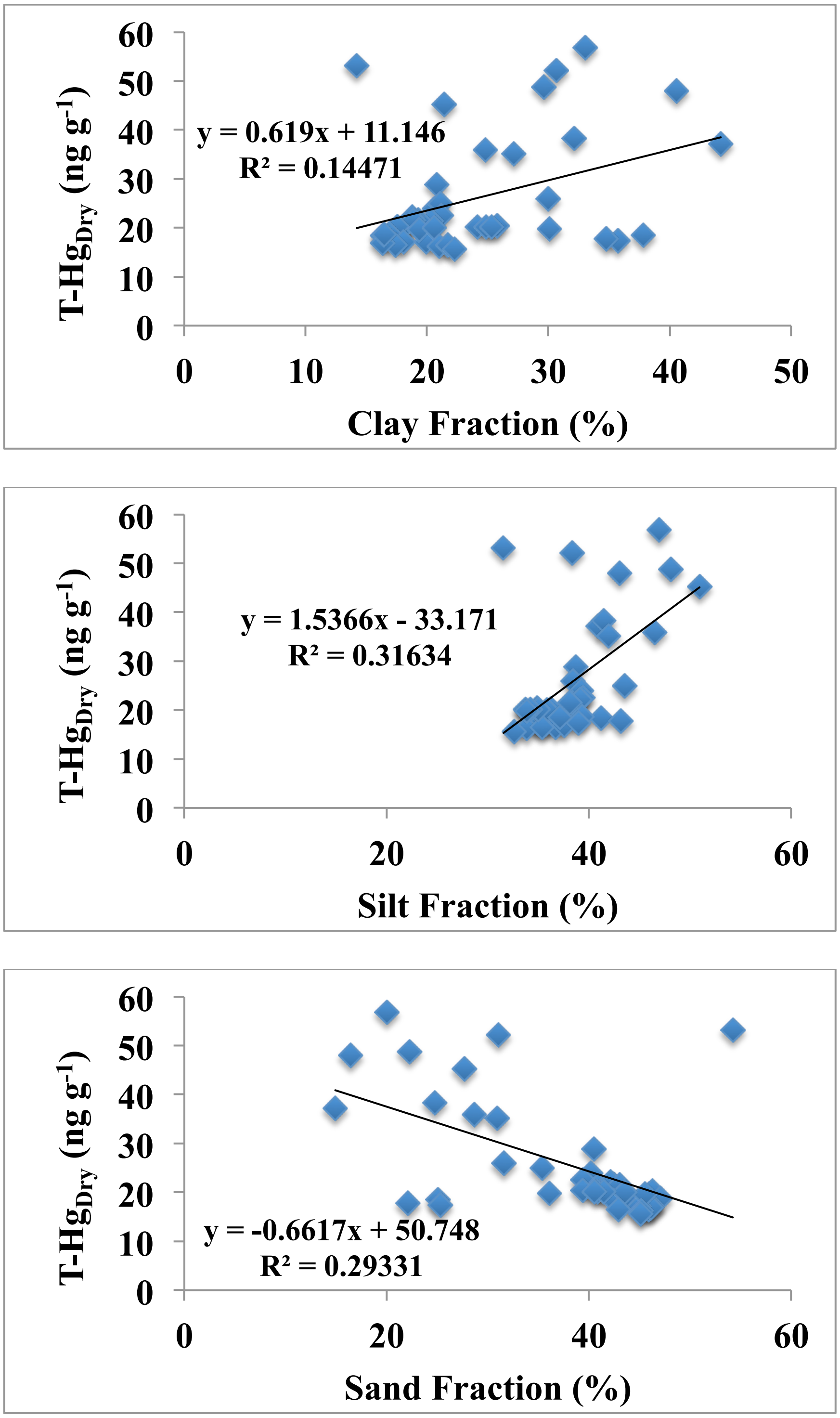

Figure B2. Correlation between Hg concentration and the percentage of grain size fraction in coring site 11 – Mid Galveston Bay.

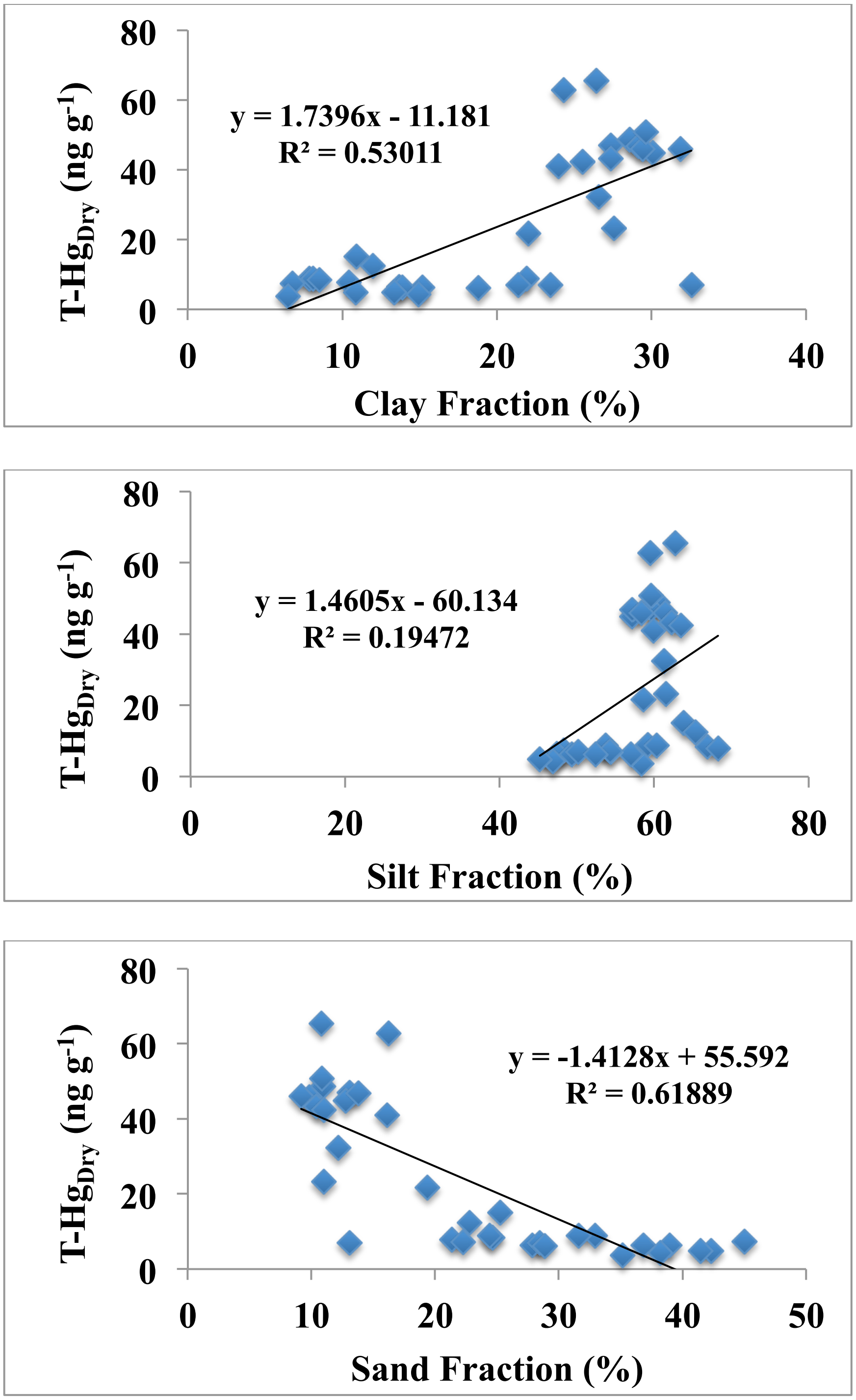

Figure B3. Correlation between Hg concentration and the percentage of grain size fraction in coring site 15 – Taylor Lake.